Supplementary Information for "Impact of dynamic sub-populations within grafted chains on the protein binding and colloidal stability of PEGylated nanoparticles."

Delyan R. Hristov,[a] Hender Lopez,[b] Yannick Ortin,[c] Kate O'Sullivan,[c] Kenneth A. Dawson,[c,*] Dermot F. Brougham[c,*]

Table of Contents

Figures

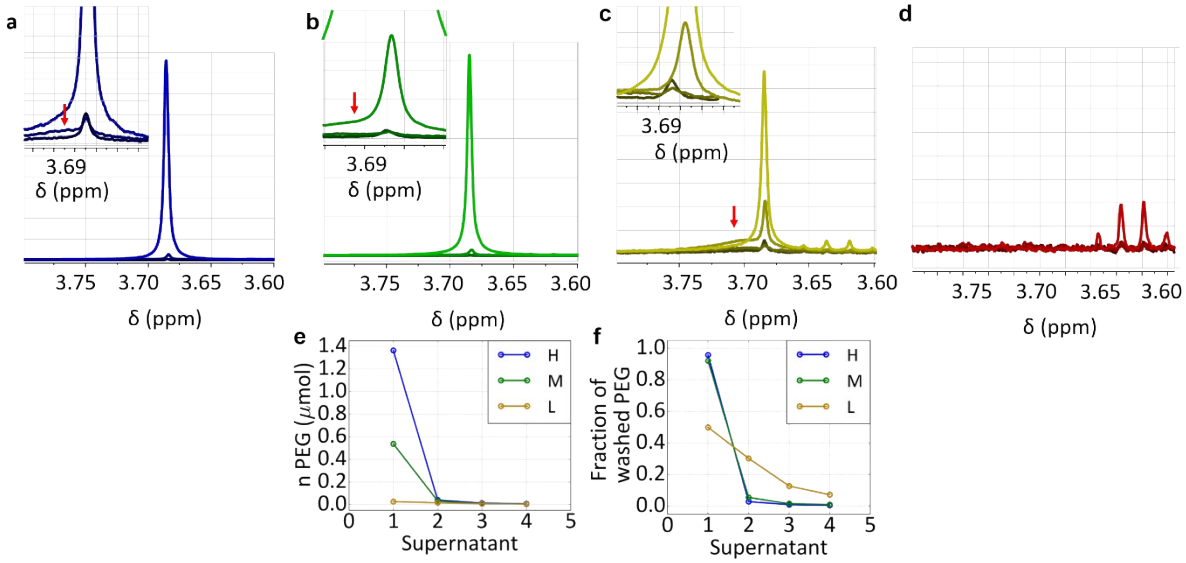

Figure S1. NMR signal of particle supernatants 1 to 4 for (a) H, (b) M, (c) L and (d) VL particles. Signal shows that majority of free PEG is lost in the first 2 washes. Some amount of particles is lost in each wash as highlighted by the red arrows in the spectra. Free PEG removal is represented as (e) n (μmol) per supernatant or (f) fraction of the total free PEG lost per supernatant.

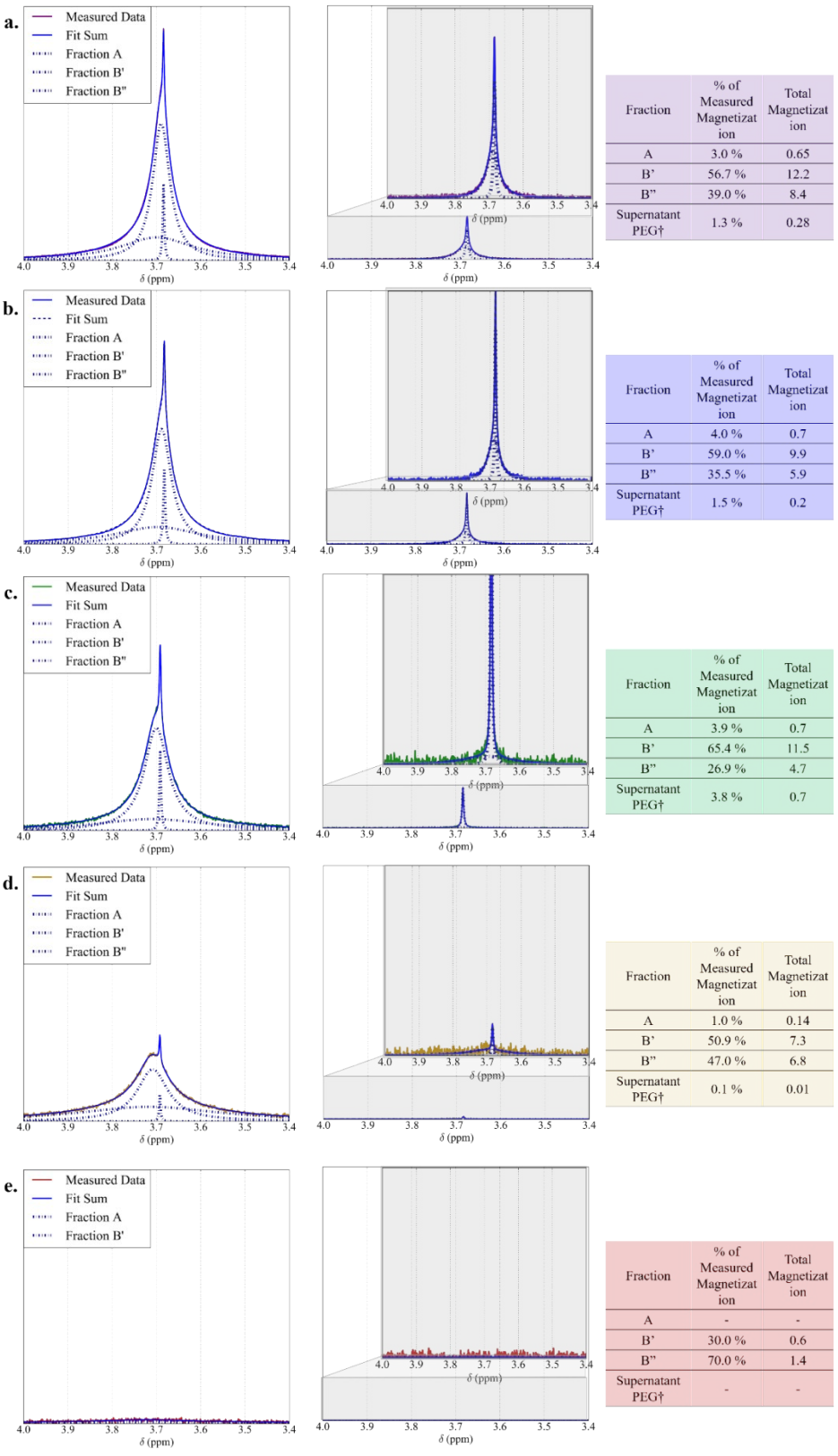

Fraction	% of Measured Magnetization	Total Magnetization
A	3.0 %	0.65
B'	56.7 %	12.2
B"	39.0 %	8.4
Supernatant PEG†	1.3 %	0.28

Fraction	% of Measured Magnetization	Total Magnetization
A	4.0 %	0.7
B'	59.0 %	9.9
B"	35.5 %	5.9
Supernatant PEG†	1.5 %	0.2

Fraction	% of Measured Magnetization	Total Magnetization
A	3.9 %	0.7
B'	65.4 %	11.5
B"	26.9 %	4.7
Supernatant PEG†	3.8 %	0.7

Fraction	% of Measured Magnetization	Total Magnetization
A	1.0 %	0.14
B'	50.9 %	7.3
B"	47.0 %	6.8
Supernatant PEG†	0.1 %	0.01

Fraction	% of Measured Magnetization	Total Magnetization
A	-	-
B'	30.0 %	0.6
B"	70.0 %	1.4
Supernatant PEG†	-	-

Figure S2. A side – by – side comparison between the PEG signal observed for the particle dispersion (left) and last supernatant (right) fit with 3 Lorentzians and 2 Lorentzians, respectively. The exact % of each fraction are provided in the tables. In the analysis it is assumed that the narrow fraction is only free PEG. Hence, as there may be some NPs remaining (the lines are broadened as compared to free PEG), the values are an overestimate.

This analysis was undertaken for representative (a) **VH**, (b) **H**, (c) **M**, (d) **L** and (e) **VL** suspensions. The specific values found varied batch – to – batch and are relatively high for the one presented. See relevant section in the SI above.

We applied a two Lorentzian fit to the signal and isolated the narrow fast moving fraction in order to estimate the PEG not associated with the particle. The signal integration obtained was further used to find the fraction of un-associated PEG from the total signal using the equation below:

$$\% = \frac{I_{supernatant\ PEG}}{I_{supernatant\ PEG} + I_{AB}} \times 100$$

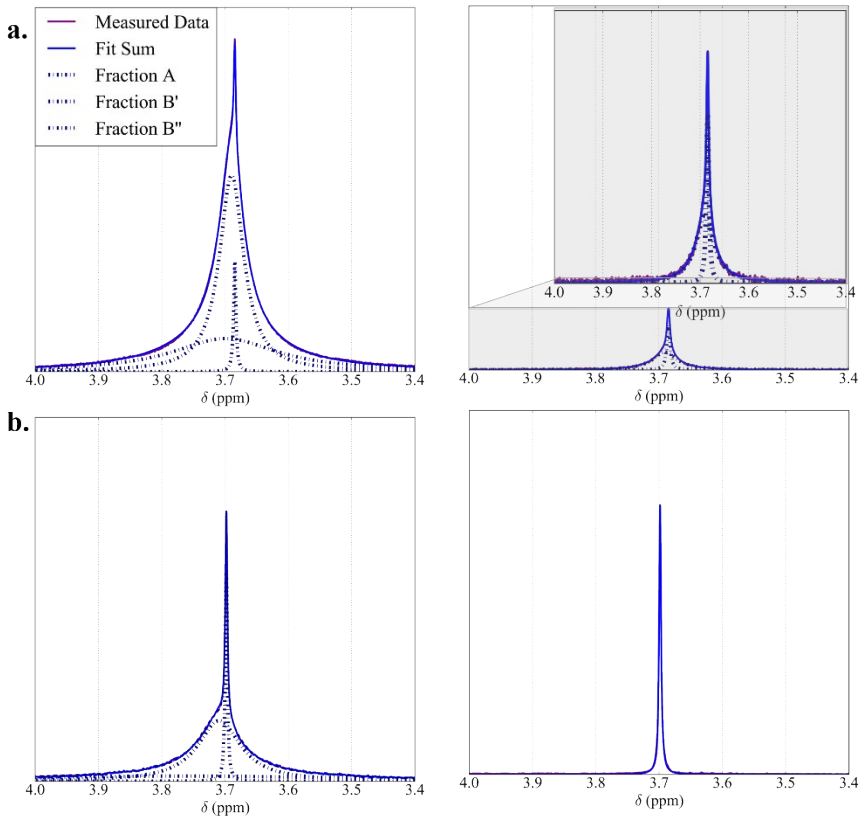

Fraction	% of Measured Magnetization	Total Magnetization
A	3.0 %	0.65
B'	56.7 %	12.2
B"	39.0 %	8.4
Supernatant PEG†	1.3 %	0.28

Fraction	% of Measured Magnetization	Total Magnetization
A	8.9 %	14.2
B'	52.8 %	84.5
B"	27.6 %	44.2
Supernatant PEG†	10.7 %	17.1

Figure S3. Side – by – side comparison between the PEG signal observed for the particle dispersion (left) and last supernatant (right) fit with 3 Lorentzians and 2 Lorentzians, respectively for the same particle batch (a) after synthesis and (b) twelve weeks later. Analysis is the same as figure S11. A significant increase in the free PEG (including a change in the line shape of the supernatant peak) is observed over this timescale, hence all data presented in the manuscript were recorded within 6 weeks.

Table S1. Measured coverage, ρ, of PEGylated silica particles. Average and standard deviations are the result of analysing at least N = 3 particle batches.

Particle Type	50 nm SiO_2 PEG 1000	50 nm SiO_2 PEG 5000	77 nm SiO_2 PEG 5000	96 nm SiO_2 PEG 5000	200 nm SiO_2 PEG 5000
VH	0.9 ± 0.2	0.35 ± 0.07	0.5 ± 0.1	0.26 ± 0.02	0.12 ± 0.02
H	0.8 ± 0.2	0.37 ± 0.06	-	-	0.07 ± 0.01
M	0.25 ± 0.07	0.28 ± 0.02			0.05 ± 0.01
L	0.07 ± 0.02	0.17 ± 0.04			0.02 ± 0.01
VL	0.05 ± 0.04	0.06 ± 0.02			0.01 ± 0.01

Note that unless explicitly stated the data shown are for suspensions of 50 nm (diameter from TEM) PEG5000 grafted NP suspensions in H_2O or D_2O.

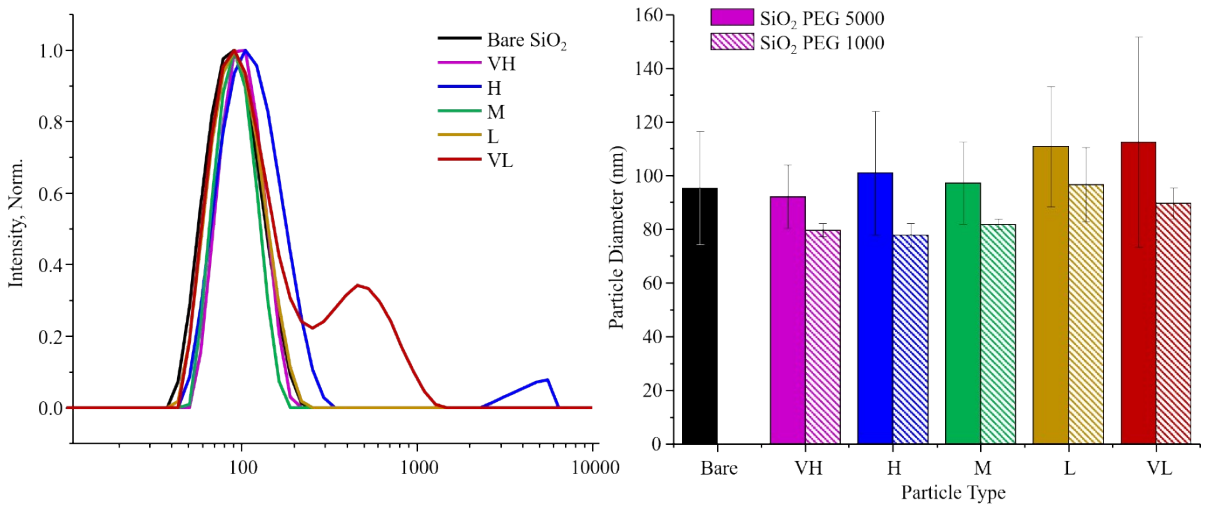

Figure S4. DLS data for representative 50 nm NP suspensions in H_2O, displayed as (a) particle intensity distribution and (b) mean Z - Average diameter.

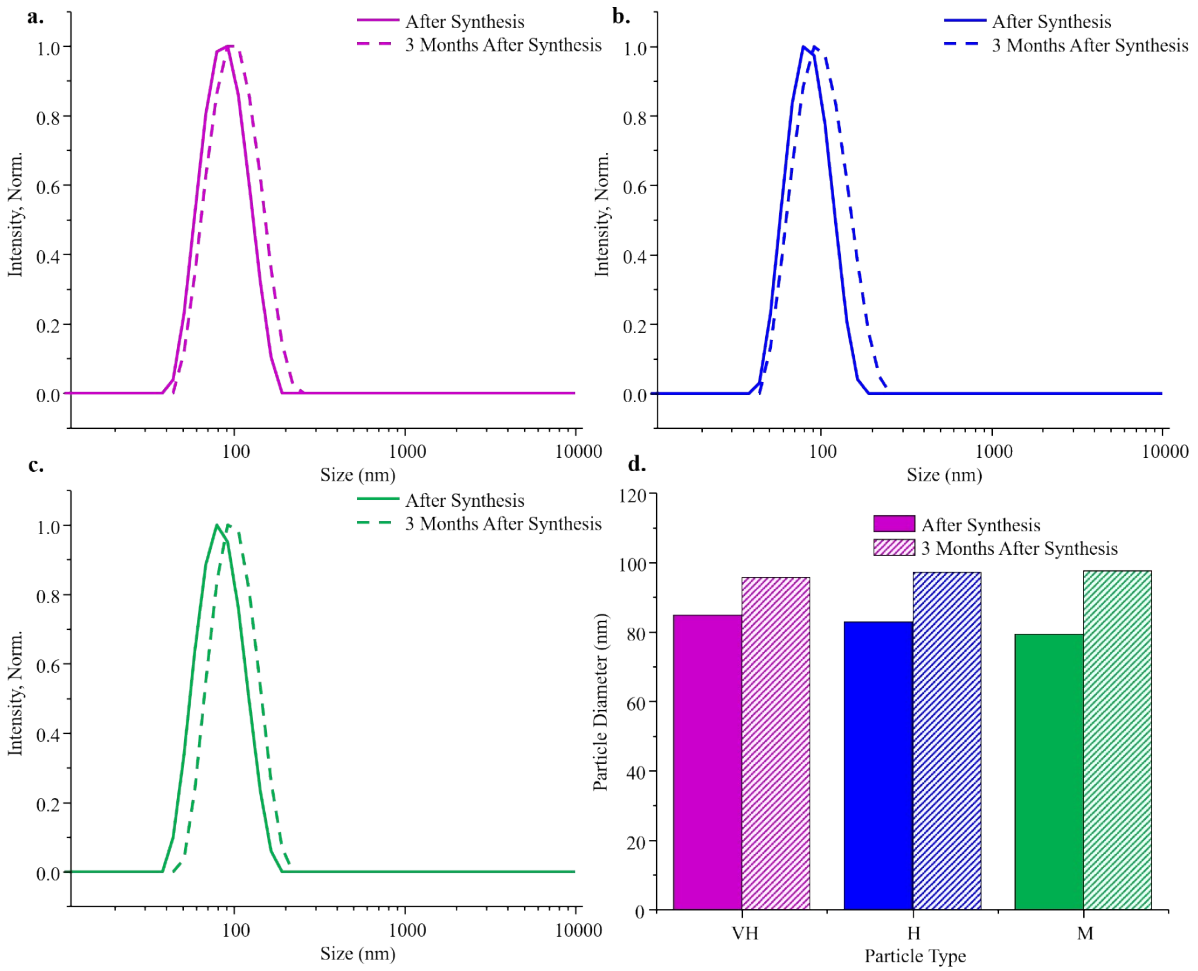

Figure S5. Stability of the same particle dispersions over time as measure by DLS particle intensity distributions for (a) **VH**, (b) **H** and (c) **M** particles, and (b) mean Z - Average diameter.

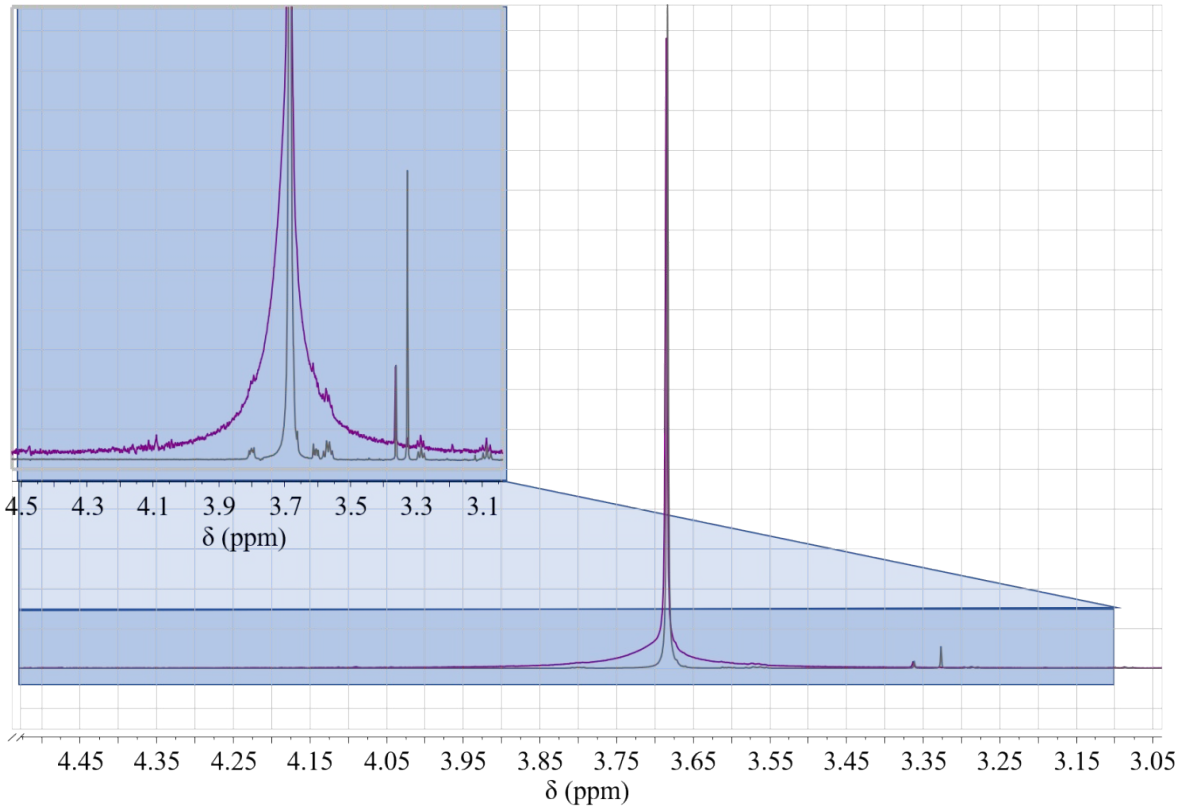

Figure S6. Spectral overlap of free PEG (grey line) and particle bound PEG (purple line) for a **VH** suspension.

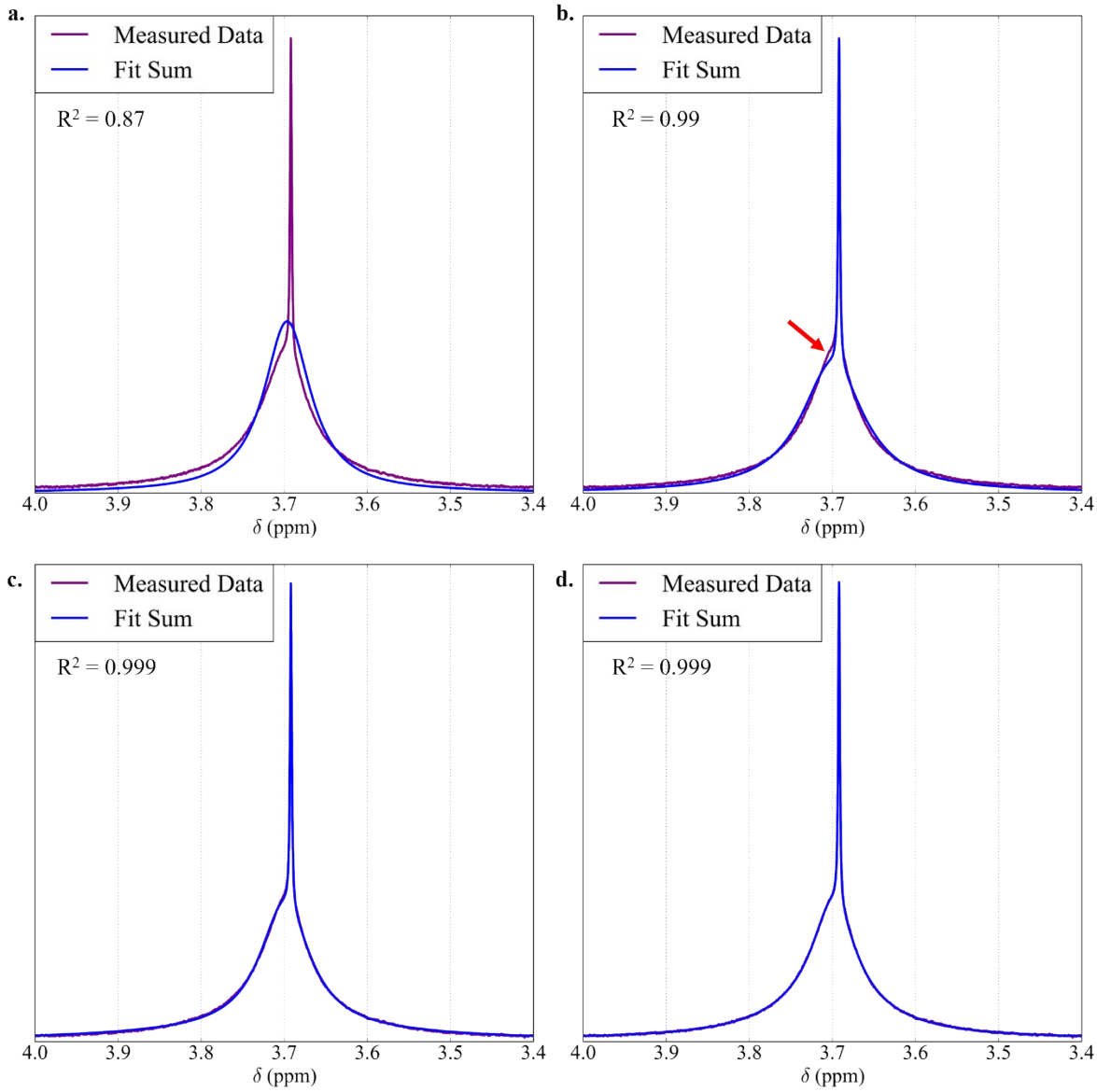

Figure S7. Evaluation of fitting strategies featuring (a) one, (b) two (c) three and (d) four Lorentzian functions, for the ^{1}H spectrum of a VH suspension. The coefficient of determination, R^2, is provided as a measure of the fitting ability. It is observed that two Lorentzians are sufficient to obtain $R^2 > 0.98$ (in most cases), the addition of a third Lorentzian provides an almost perfect agreement, adding more functions make no discernible further improvement.

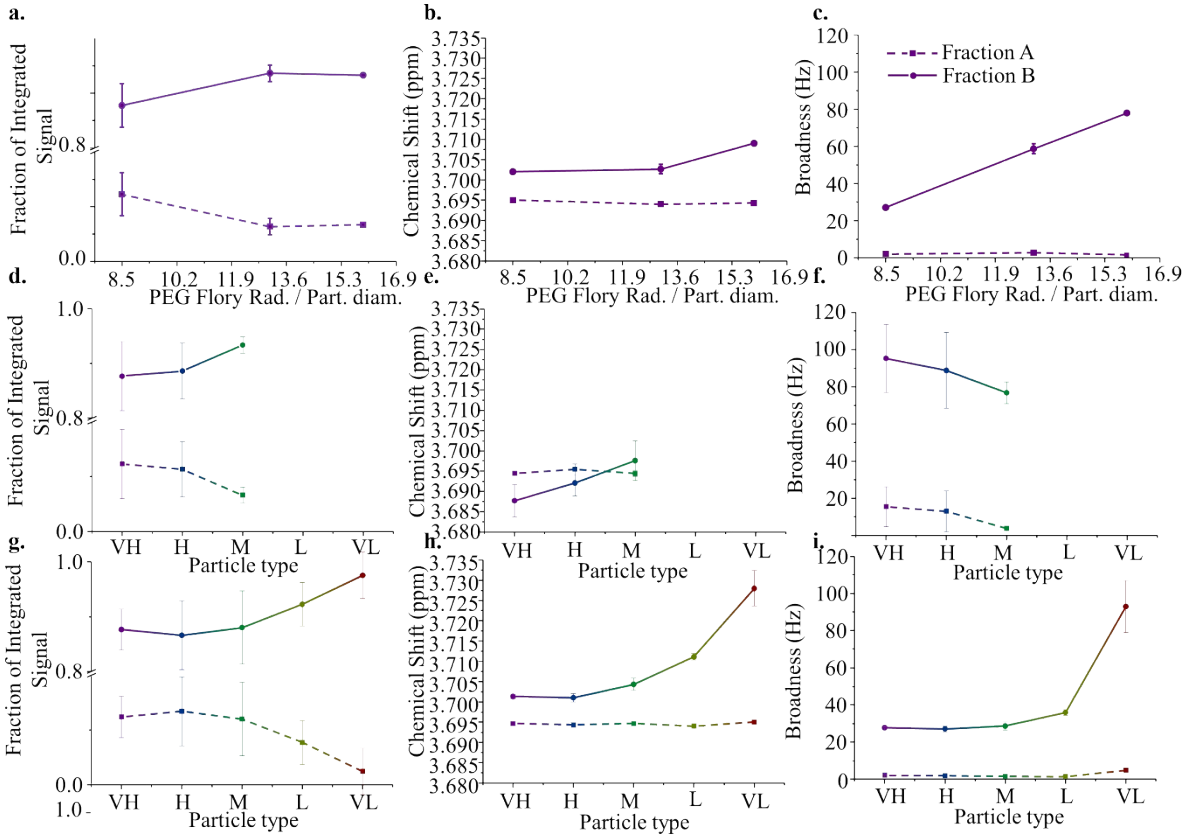

Figure S8. (a) Fraction of signal, (b) chemical shifts and (c) broadness of fraction ***A*** and ***B*** with (a – c) change of the PEG / particle size ratio and PEG coverage for a given ratio, for (d – f) PEG 1000 and (f – i) 5000.

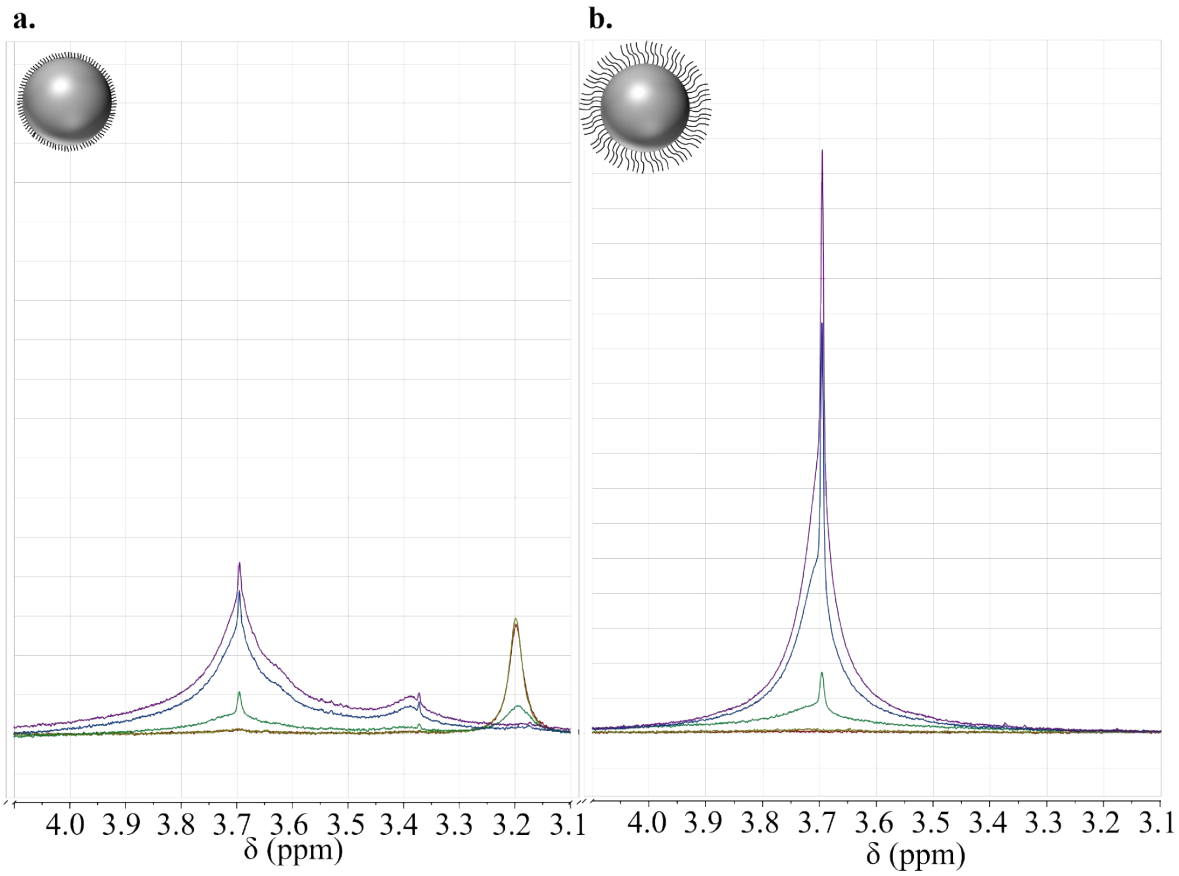

Figure S9. A representative set of ^{1}H spectra for 50 nm NPs with varying coverage of (a) PEG 1000 and (b) PEG 5000. The schematics in the top left corners represent the relative PEG/particle size for fully extended molecules.

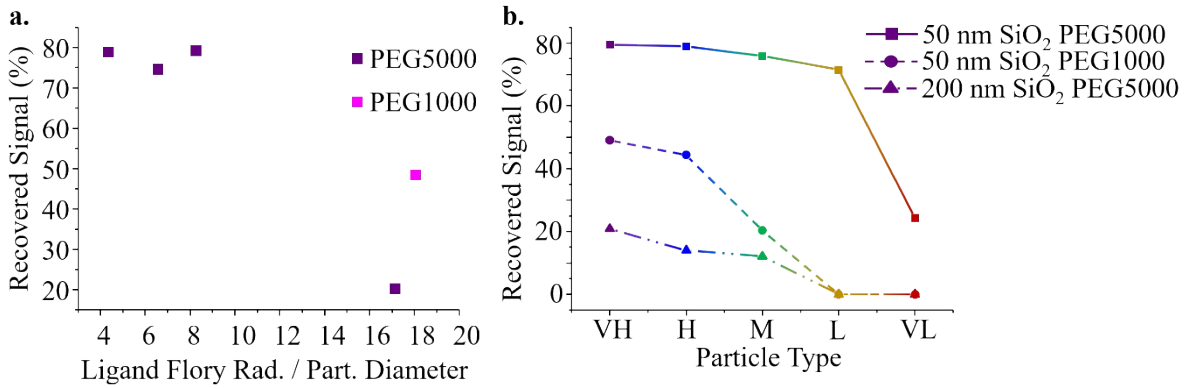

Figure S10. (a) change in the recovered signal (%) with PEG/ particle size ratio of VH only (b) and all samples.

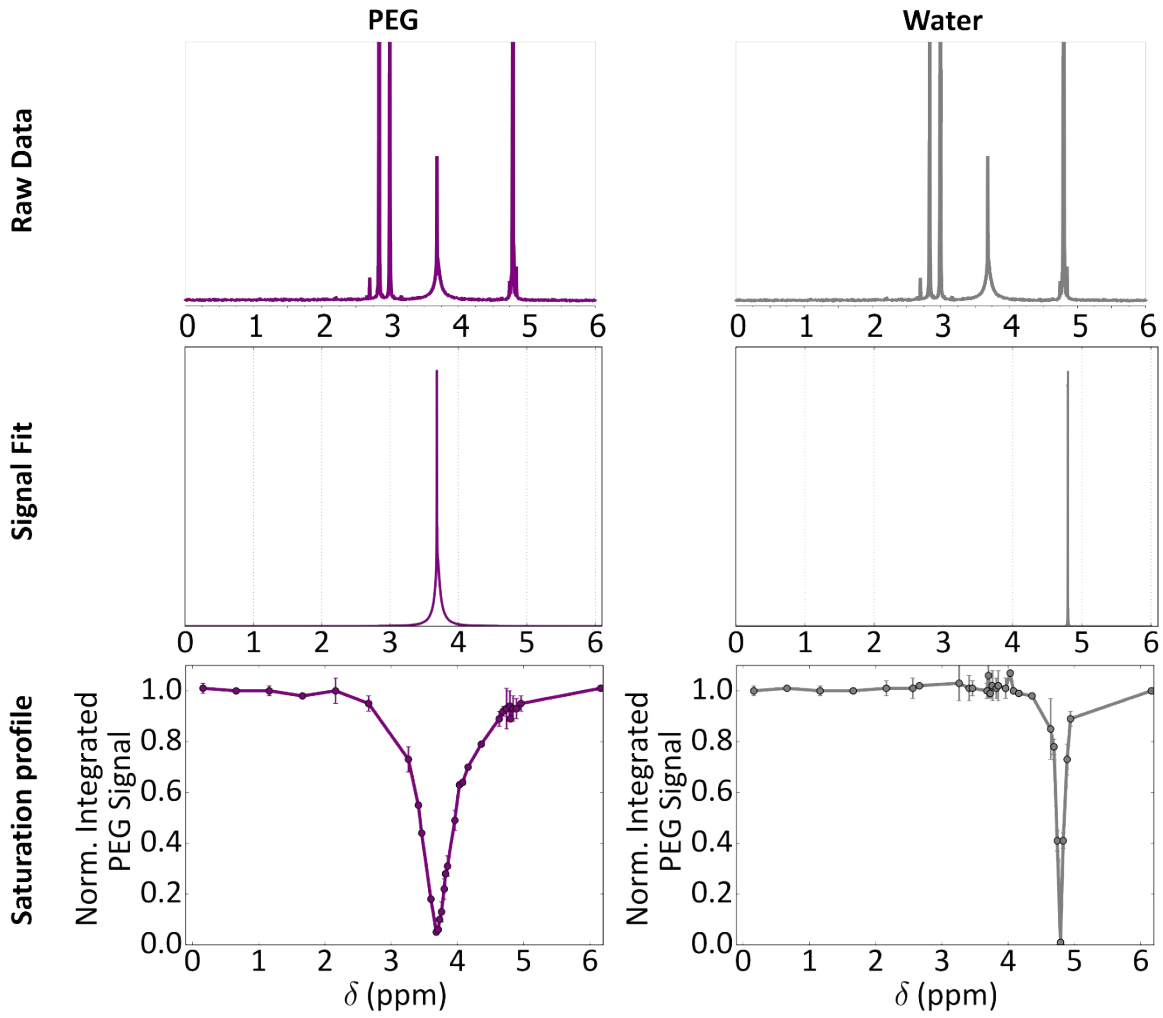

Figure S11. Raw data, fit peak and saturation profiles of VH particles. The PEG (purple) and water (grey) peaks were fit. Error bars in the saturation profiles are averaged from N = 3 and N = 4 independent particle batches, respectively. The error bars represent the standard deviation.

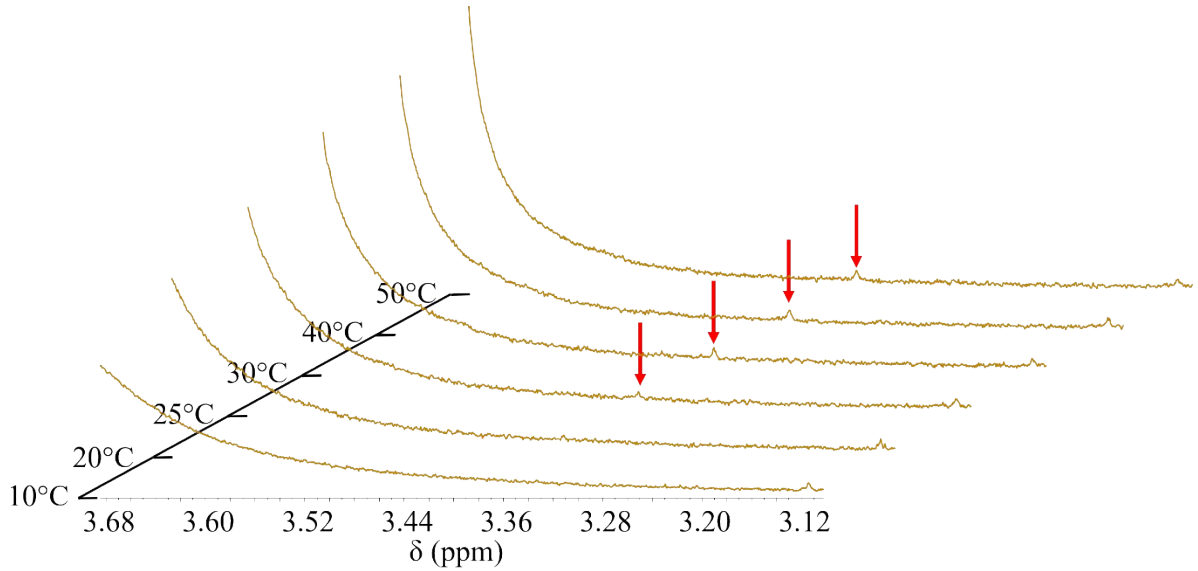

Figure S12. Appearance of the resonance (red arrow) assigned to the methoxy end group of the grafted PEG molecules for a ***L*** suspension on increasing the temperature, see main text.

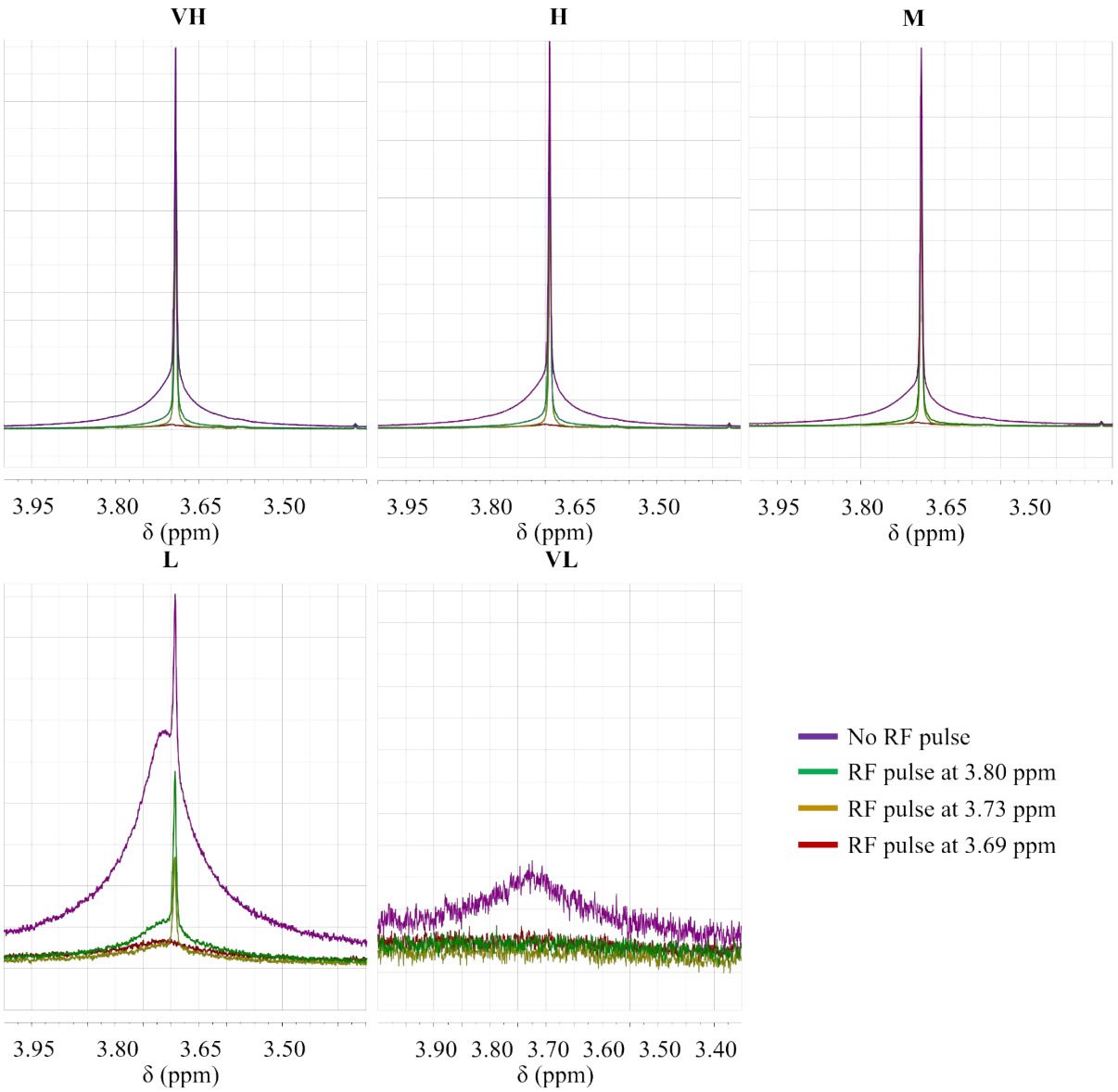

Figure S13. Hole burning experiment for **VH - VL** samples at 3.8 ppm (green line), 3.73 ppm (yellow line) and 3.69 (red line). The FWHM of the selective pulse was 14 Hz (0.023 ppm).

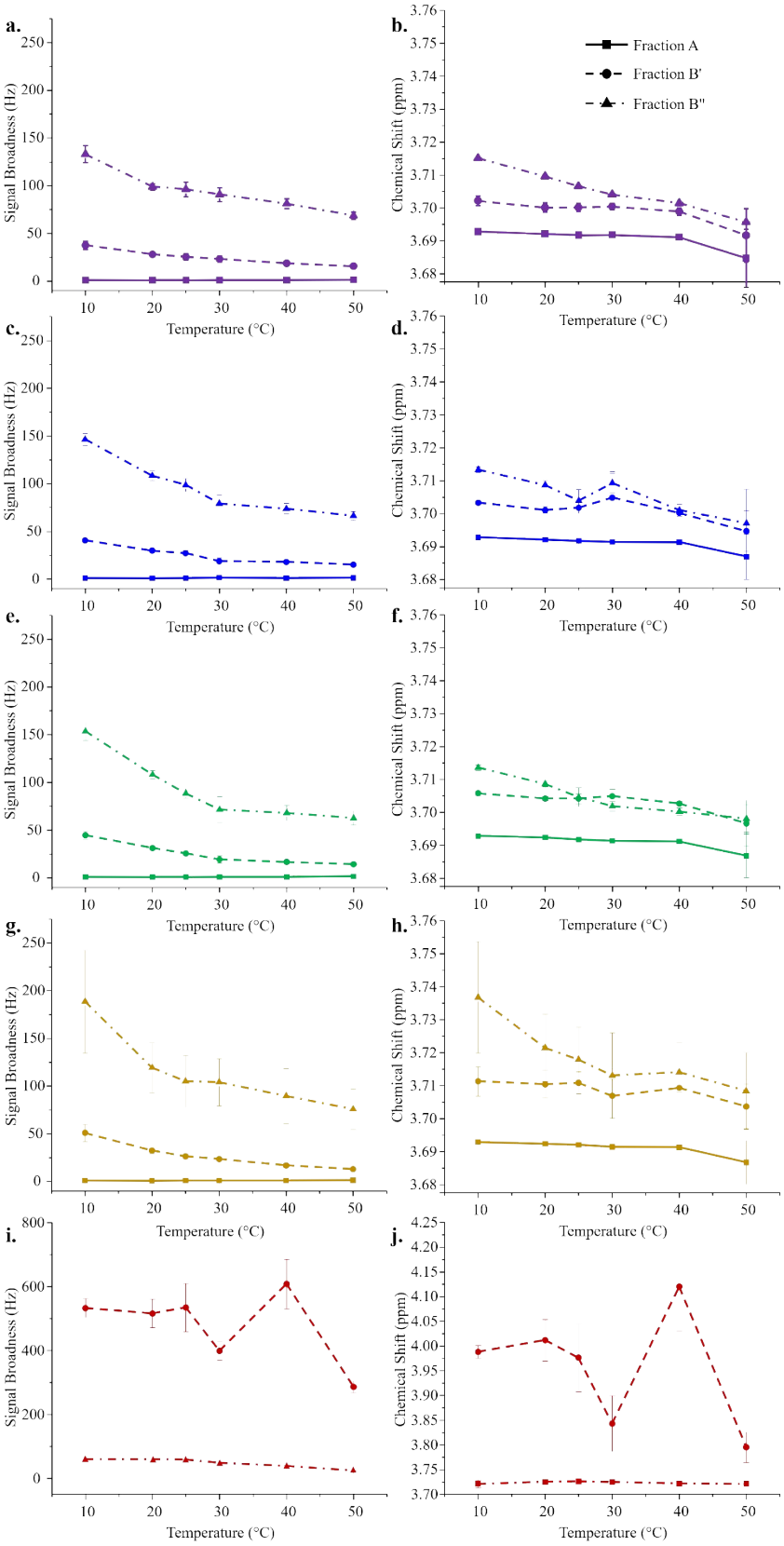

Figure S14. Signal broadness and chemical shift for fractions ***A***, ***B'*** and ***B"*** resulting from a three Lorentzian fitting of the ^{1}H PEG signal in the range of 10 – 50 °C for **VH** (a and b), **H** (c and d), **M** (e and f), **L** (g and h) and **VL** (i and j).

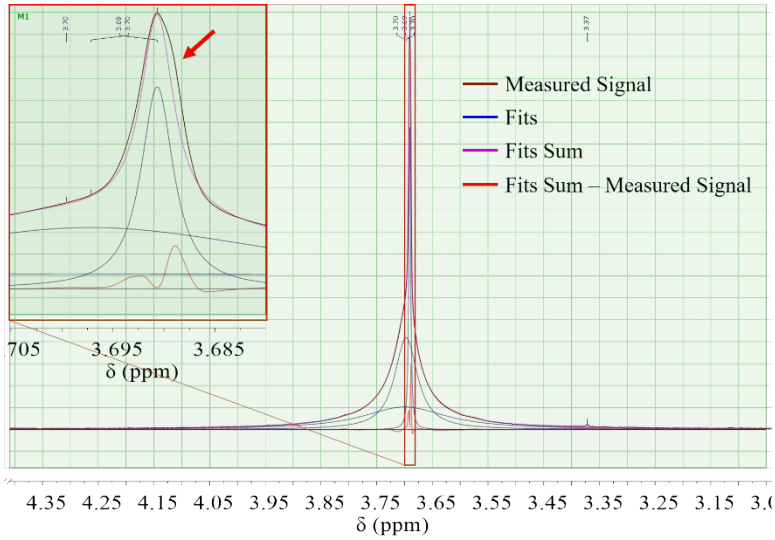

Figure S15. Example spectra showing subfractions of ***A*** appearing at high temperature in a **VH** sample.

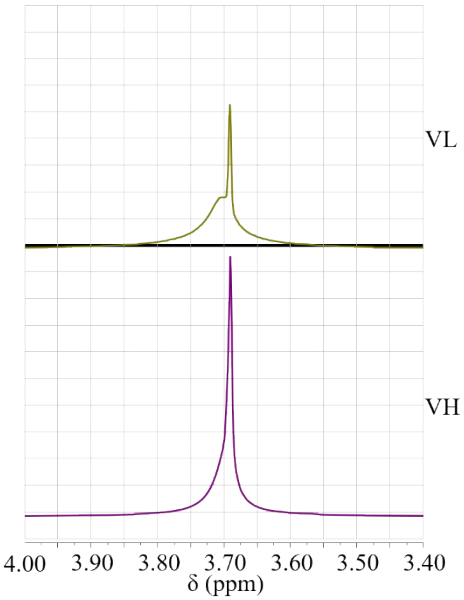

Figure S16. NMR spectra of **VL** and **VH** SiO_2 PEG particles in D_2O at 50°C.

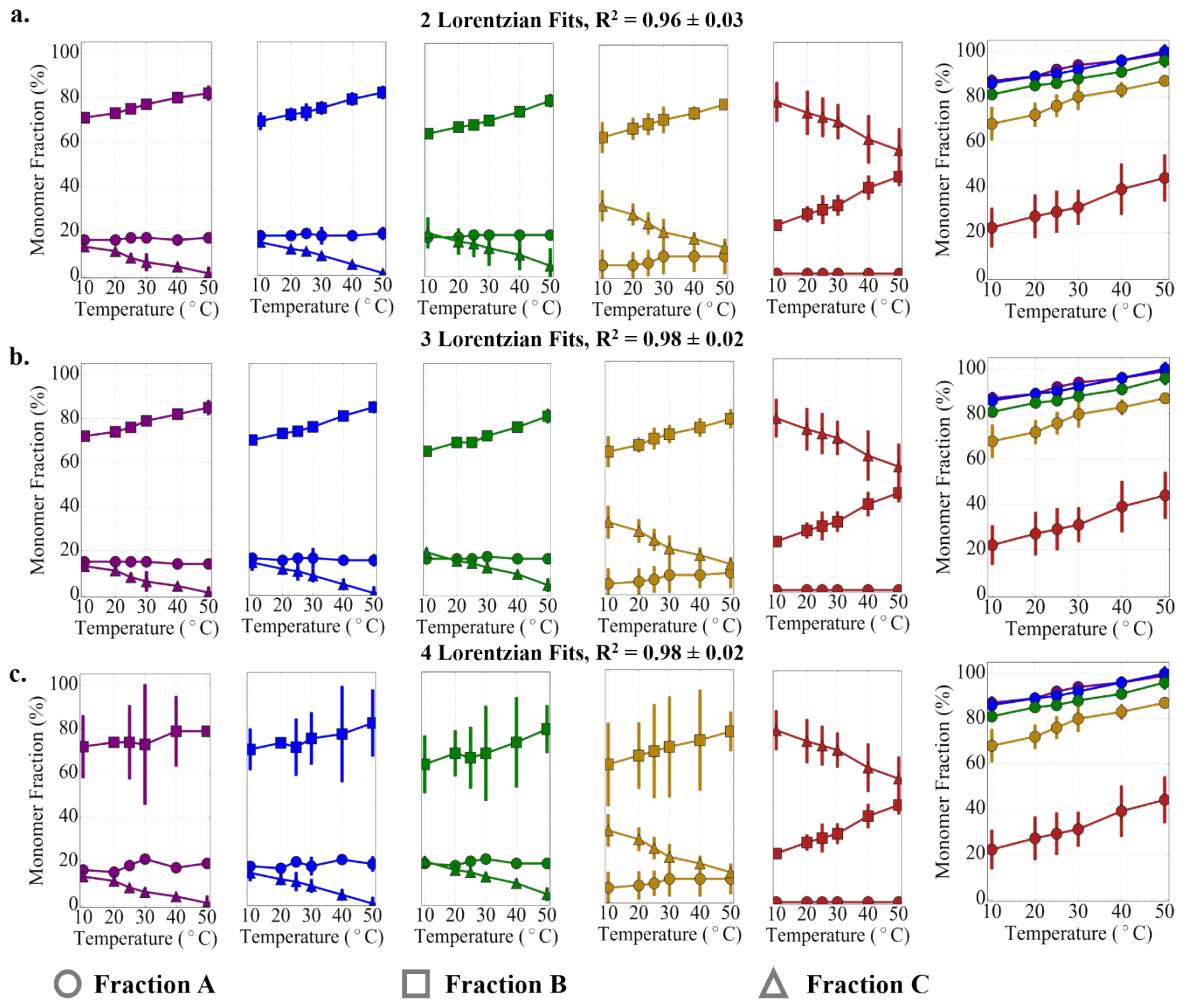

Figure S17. Analysis of the data used for figure 2 (main paper) using (a) 2, (b) 3 and (c) 4 Lorentzians. Signal fitting was ≥ 90% for 2 Lorentzians, ≥ 97% for 3 Lorentzians and ≥ 99% for 4 Lorentzians. Increasing the number of functions makes almost no discernible difference to the quantitation (supporting the assignment of three fractions A, B and C), but increases the error estimates.

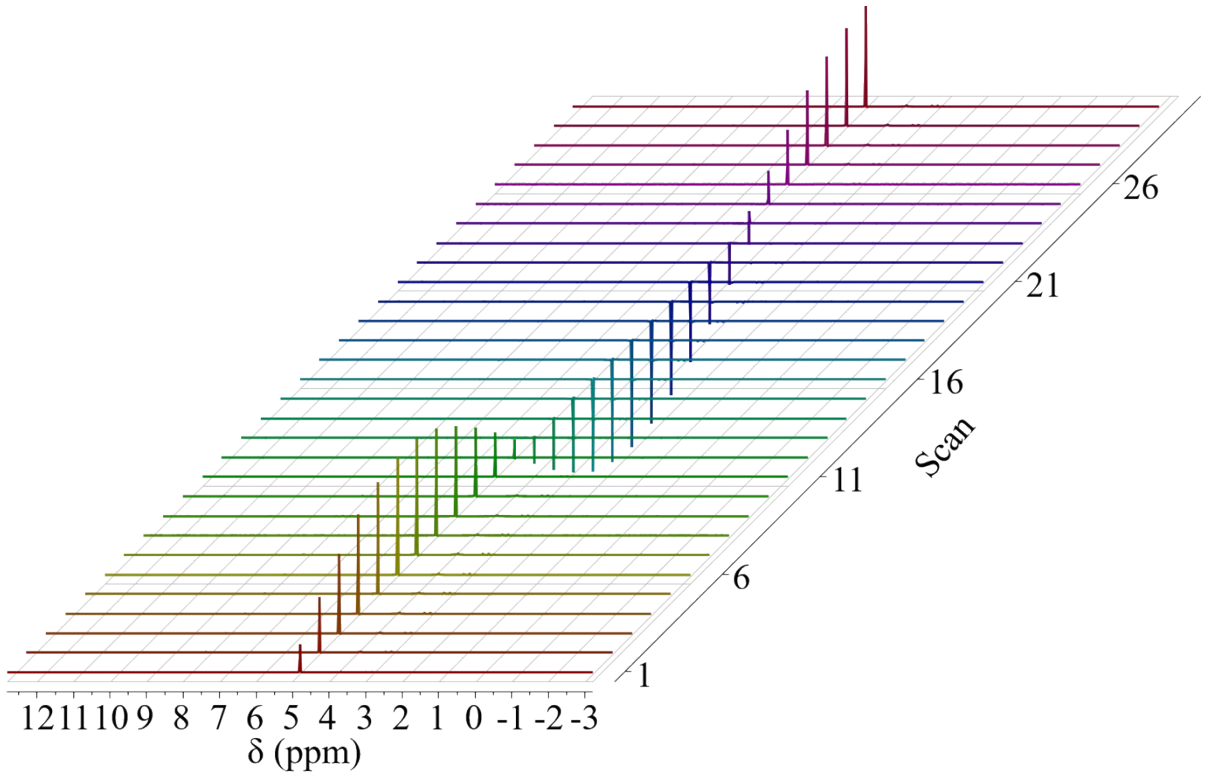

Figure S18. Representative 180º pulse calibration data. This check was performed before most reported CPMG experiments, but was always found to be the same.

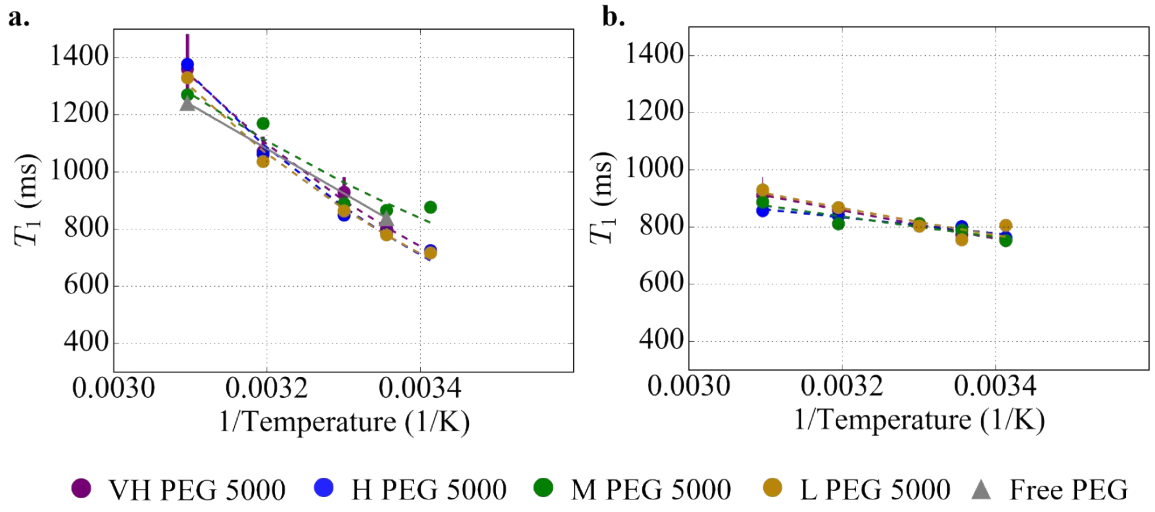

Figure S19. T_1 values measured for (a) fraction ***A*** and (b) fraction ***B*** as a function of temperature and coverage. All experiments consisted of 100 spectra with a Tau = 100 ms and were fitted with a mono-exponential function.

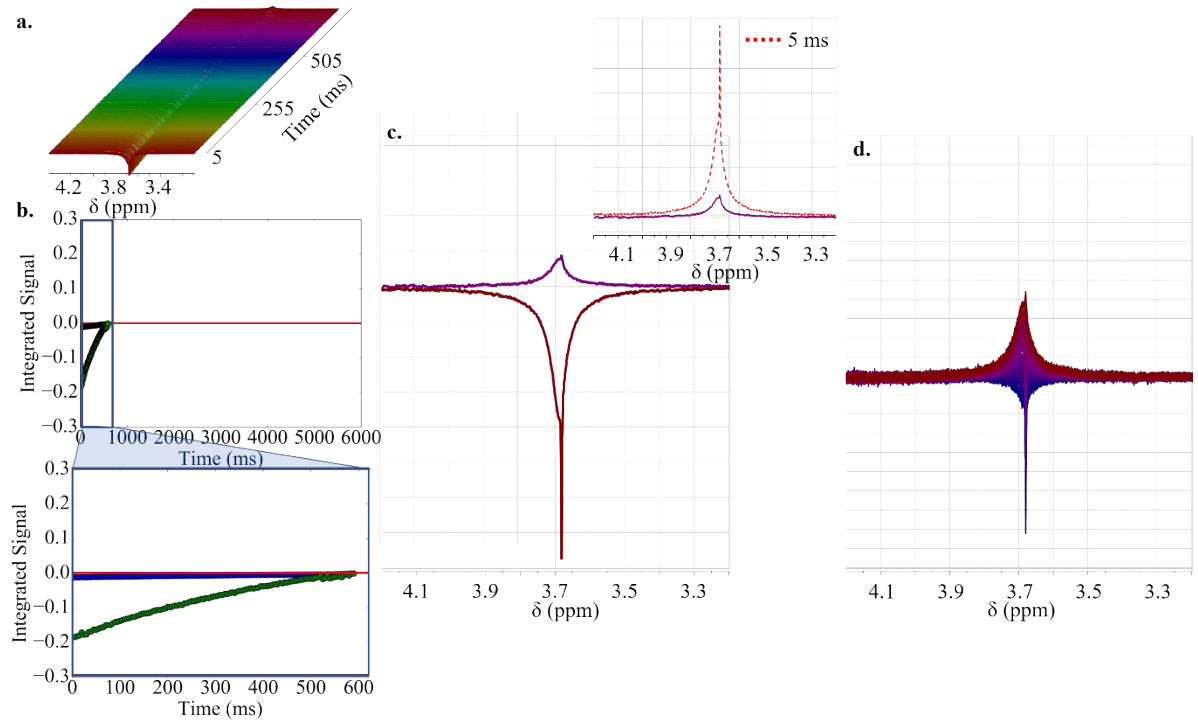

Figure S20. The outcome of an inversion recovery experiment with an initial Tau of 5 ms. Data recorded as a function of Tau are shown as a (a) stacked spectra and (b) integrals. (c) The first and last spectra in the experiment, with the former inverted in the insert for comparison. (d) Spectra recorded at close to the null. See discussion below.

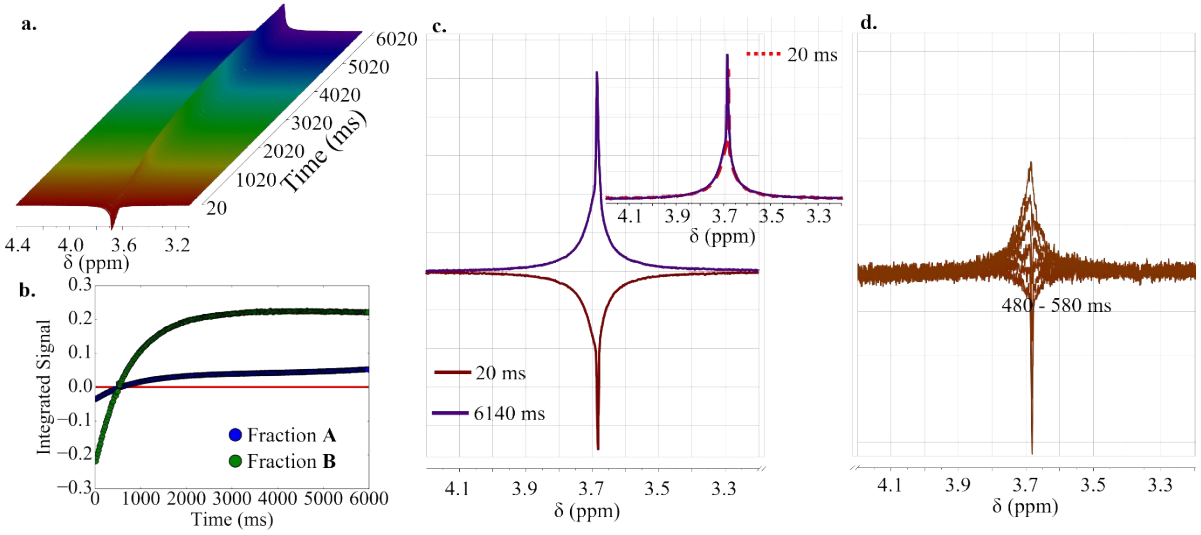

Figure S21. The outcome of an inversion recovery experiment with an initial Tau of 20 ms. Data recorded as a function of Tau are shown as a (a) stacked spectra and (b) integrals. (c) The first and last spectra in the experiment, with the former inverted in the insert for comparison. (d) Spectra recorded at close to the null. See discussion below.

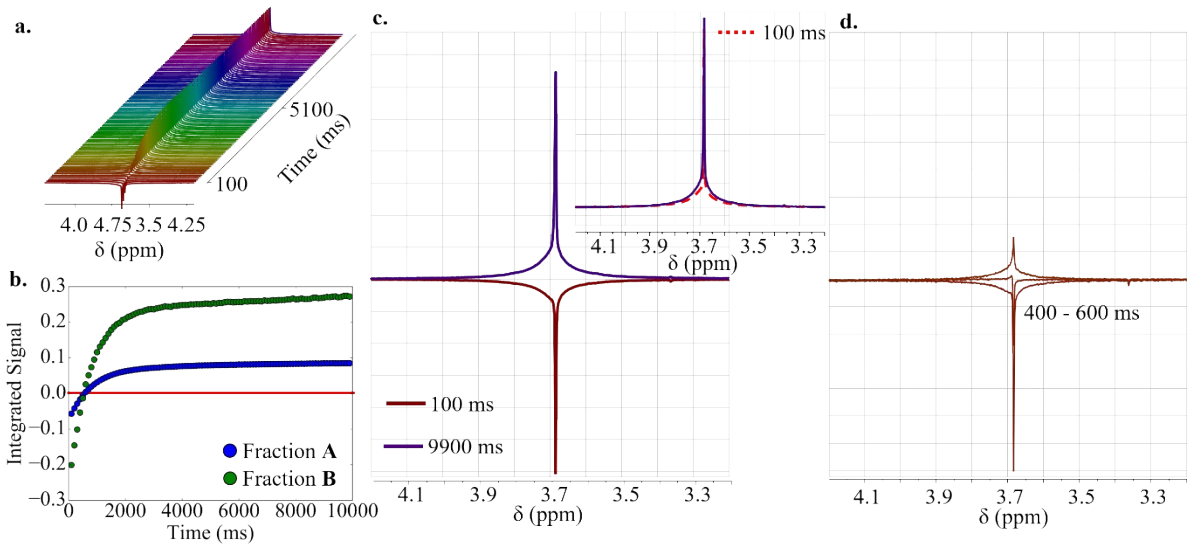

Figure S22. The outcome of an inversion recovery experiment with an initial Tau of 100 ms. Data recorded as a function of Tau are shown as a (a) stacked spectra and (b) integrals. (c) The first and last spectra in the experiment, with the former inverted in the insert for comparison. (d) Spectra recorded at close to the null.

Figures S20-S22 confirm that the lineshape is almost completely independent of Tau, and hence both fractions ***A*** and ***B*** have long, comparable, T_1 values.

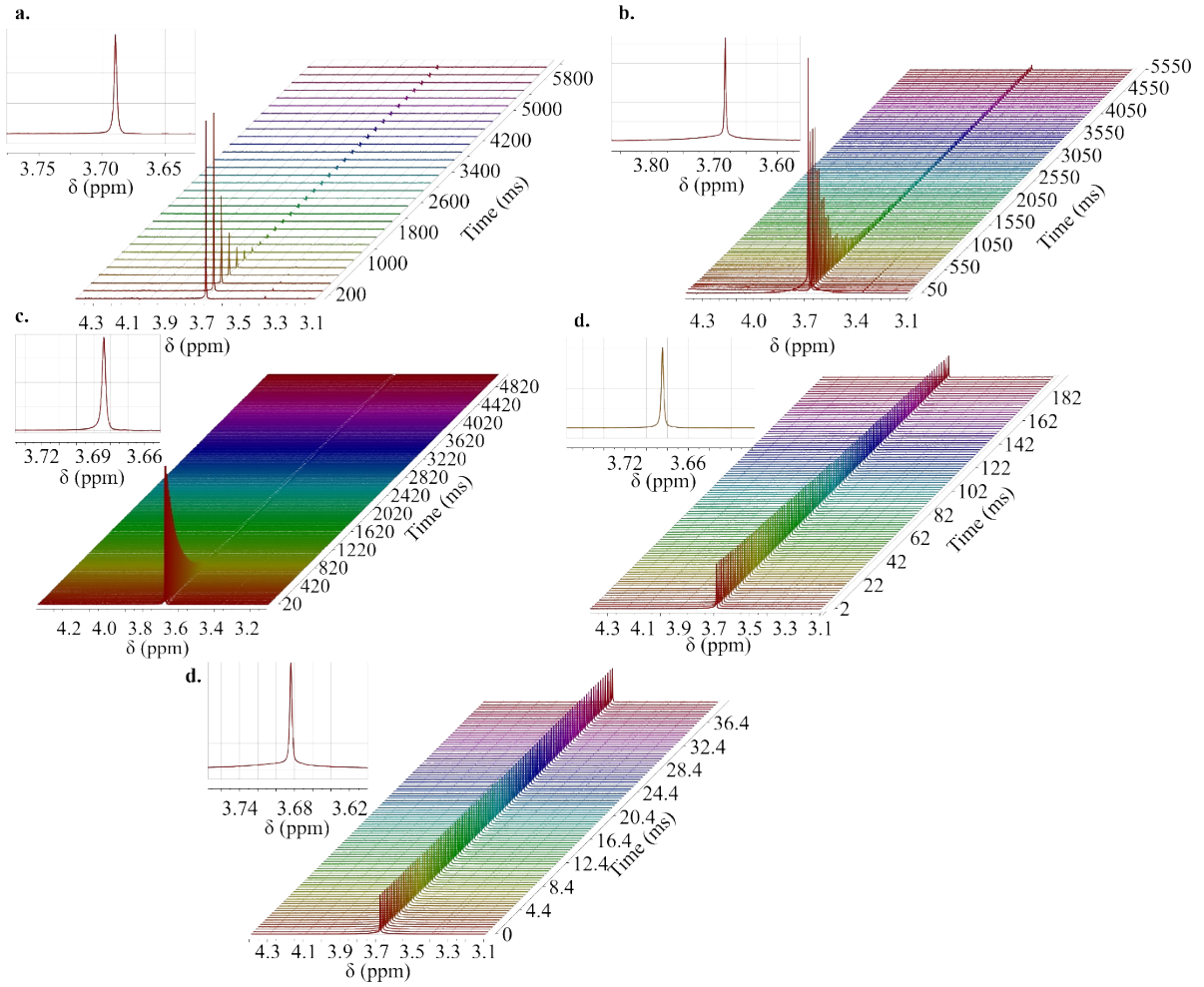

Figure S23. Echo evolution during a typical CPMG experiment for a **VH** suspension, recorded using Tau values of (a) 100, (b) 50, (c) 10, (d) 1, and (e) 0.1 ms. Figure is interpreted in the SI section below and in the main text.

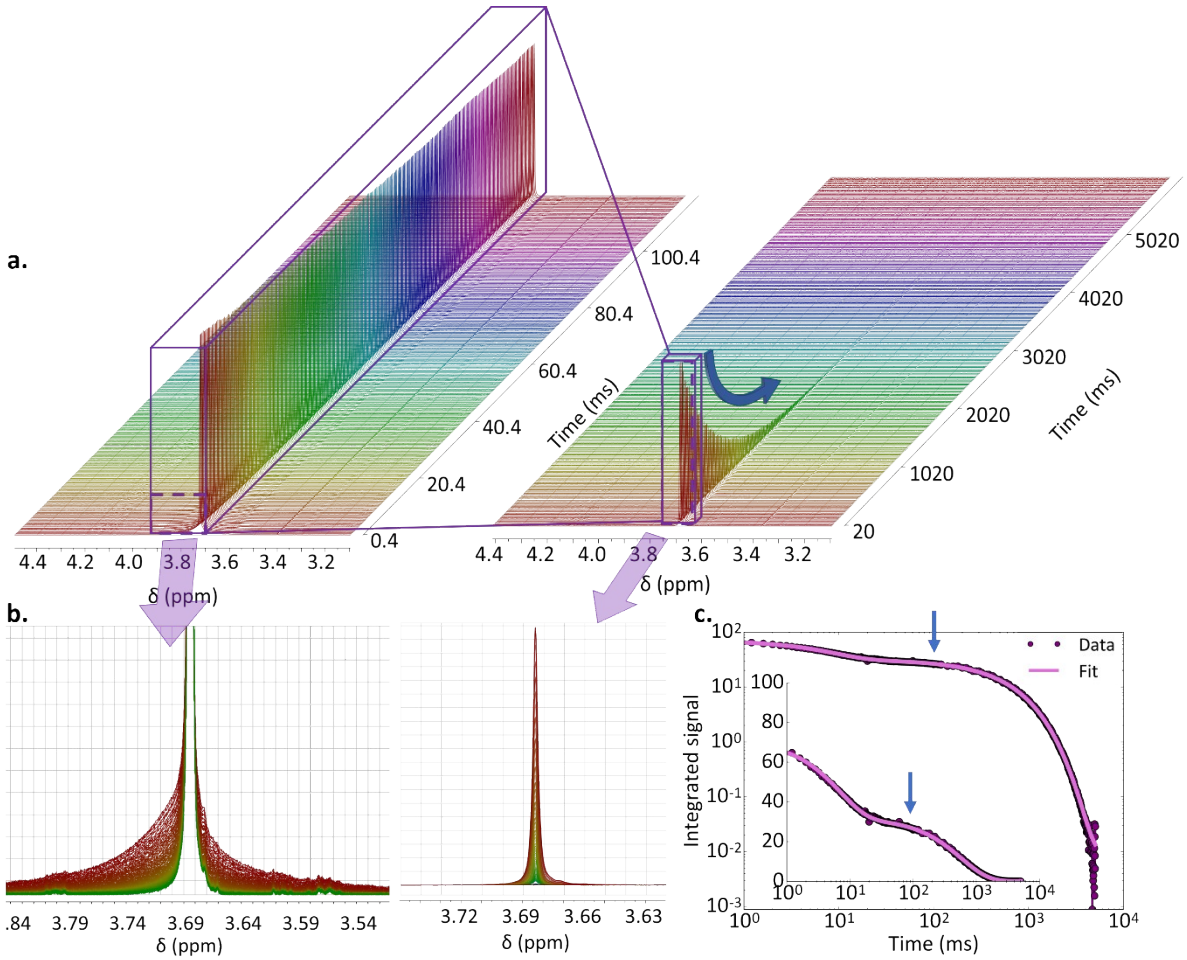

Figure S24. Spin-spin relaxation analysis of **VH** SiO_2 nanoparticle suspensions. (a) Representative CPMG echo trains recorded using echo delays of 0.1 ms (left) and 10 ms (right), for a 50 nm PEG5000-grafted (**VH**) NP suspension at 25°C. (b) The corresponding stack-plotted spectra highlight that most of the signal loss is due to the relaxation of fraction *B* at early times and *A* at a later stage. (c) Log – log and (inset) log – linear plots of the signal decay. Two separate exponential decays are observed, with the transition indicated with an arrow.

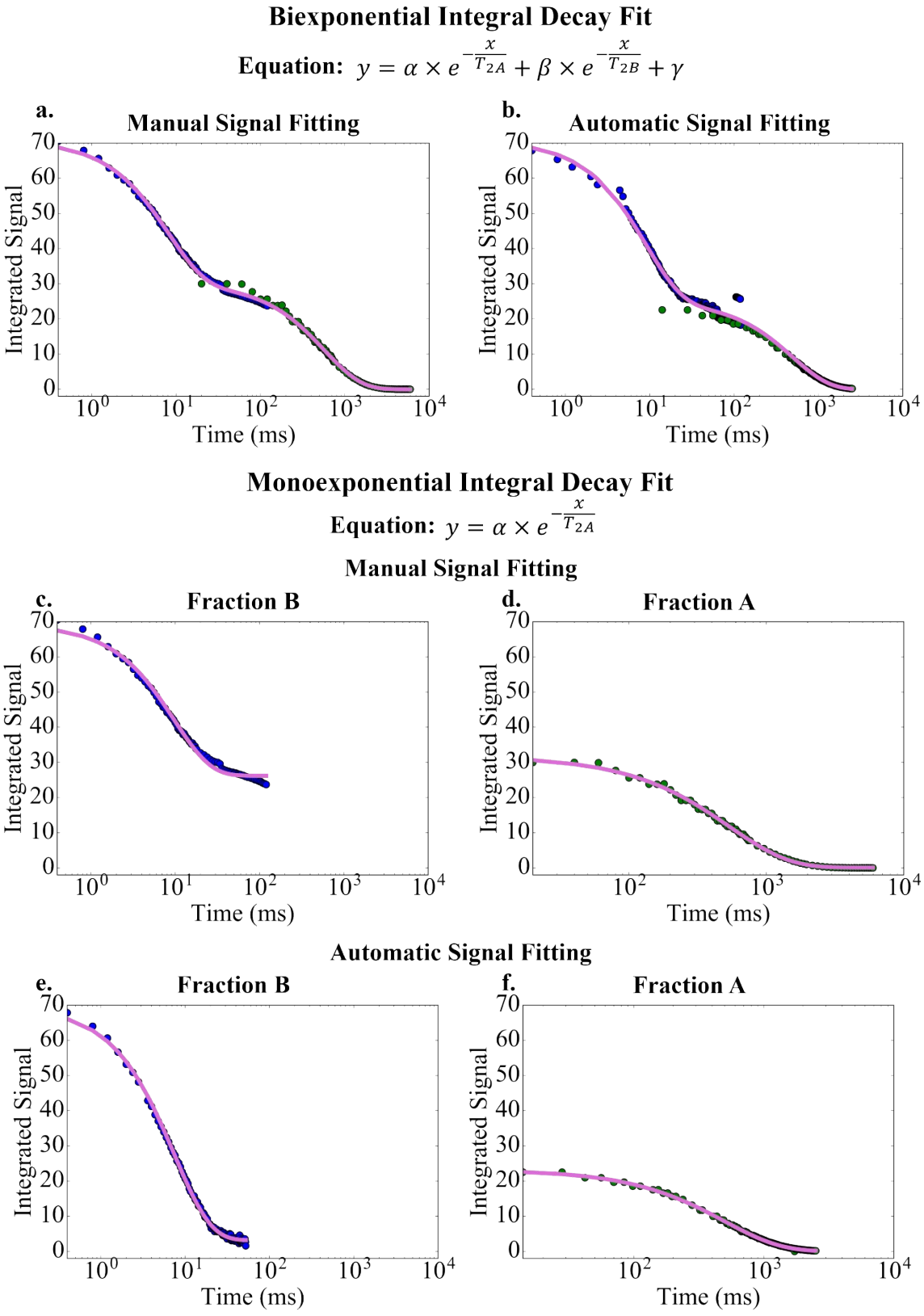

Figure S25. A representative set of graphs showing the fitting strategies for a **VH** suspension recorded at 20°C (blue circles Tau = 0.1 ms, green Tau = 10 ms), showing analysis using bi-exponential and mono-exponential decay fits obtained automatically or manually. Top panels show the biexponential decay fit of (a) manual and (b) automatic fitting. Middle panels show

monoexponential fitting of the manually obtained integration trend of fraction (c) B, from a 0.1 ms CPMG experiment and (f) A, from a 10 ms CPMG experiment. Bottom panels show the monoexponential fitting of the automatically obtained integration trend of fraction (e) B, from a 0.1 ms CPMG experiment and (f) A, from a 10 ms CPMG experiment. This confirms the suitability of the automated approach for extracting T_2 values for both fractions.

Table S2. Tabulated T_2 values from the analysis in Figure S19 showing the fitting error and R^2. The lowest errors and highest R^2 was obtained using an automatic monoexponential strategy. Table shows the relative insensitivity of the final result to the fitting method.

Signal Fitting	**Integral Decay Fitting**	$T_{2\,L}$	$T_{2\,B}$	**R^2**	
				A	**B**
Manual	Biexponential	576 ± 9	8.0 ± 0.1	0.998	
Manual	Monoexponential	539 ± 6	9.8 ± 0.2	0.999	0.998
Automatic	Biexponential	495 ± 26	8.9 ± 0.3	0.975	
Automatic	Monoexponential	498 ± 2	7.5 ± 0.05	0.999	0.998

Table S3 Dynamic parameters extracted using a standard BPP model to fit the T_1 and T_2 data (simultaneously), showing unacceptable uncertainties, as expected in the absence of a T_1-minimum

	Component **A**		Component **B**	
	E_a	E_a Fitting Error	E_a	E_a Fitting Error
VH	1974	133	753	608
H	2122	172	630	24313
M	1394	291	446	115
L	1994	139	578	185

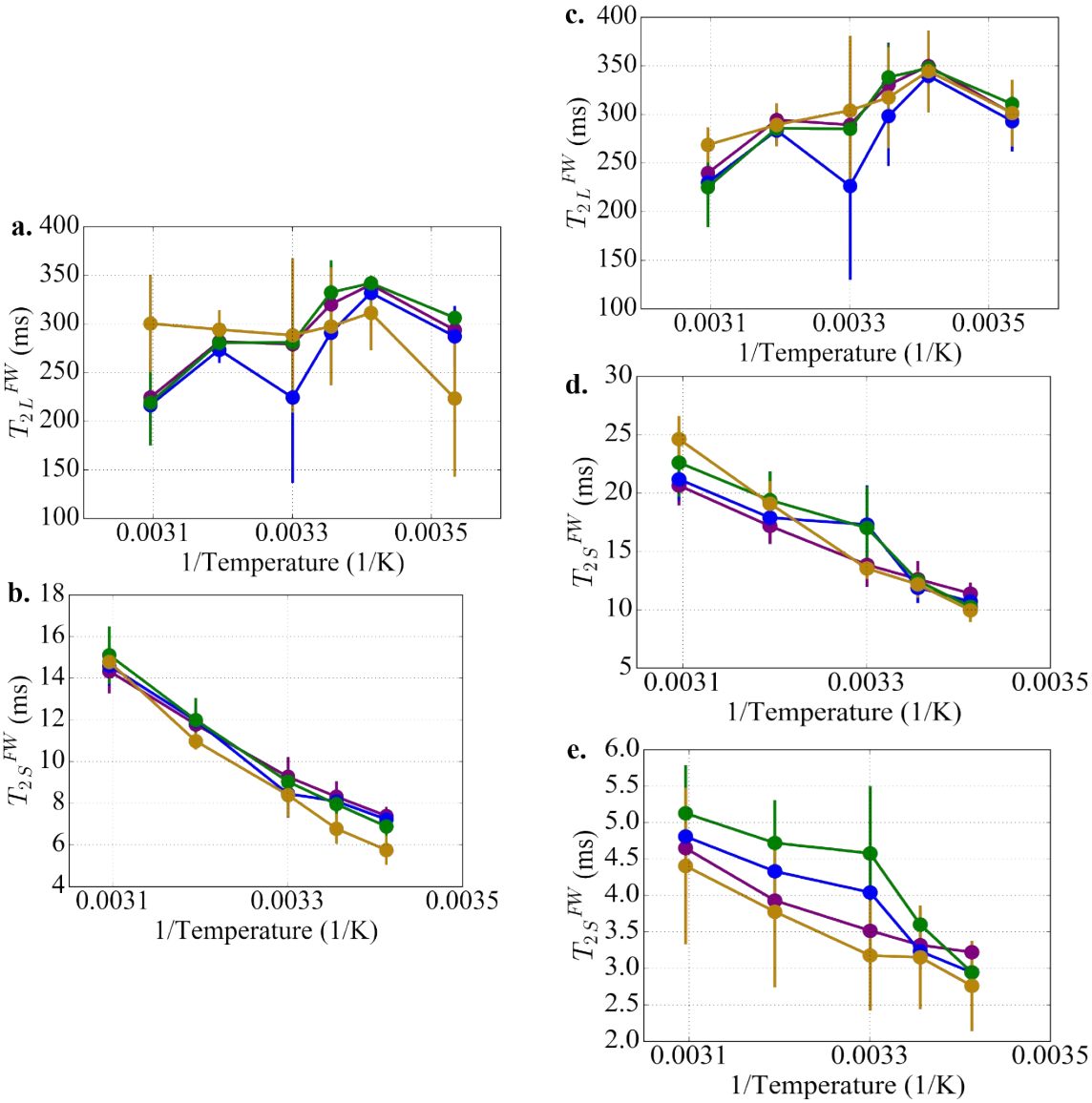

Figure S26. T_2^{FW} values calculated from the FWHM of the ^{1}H NMR spectra. Signals were fitted using either; a two Lorentzian approach to calculate the T_2^{FW} of fractions (a) **A**, and (b) **B** or; a three Lorentzian approach to calculate the T_2^{FW} for fractions (c) **A**, (d) **B'** and (e) **B"**. The error bars are the result of averaging N = 3 samples.

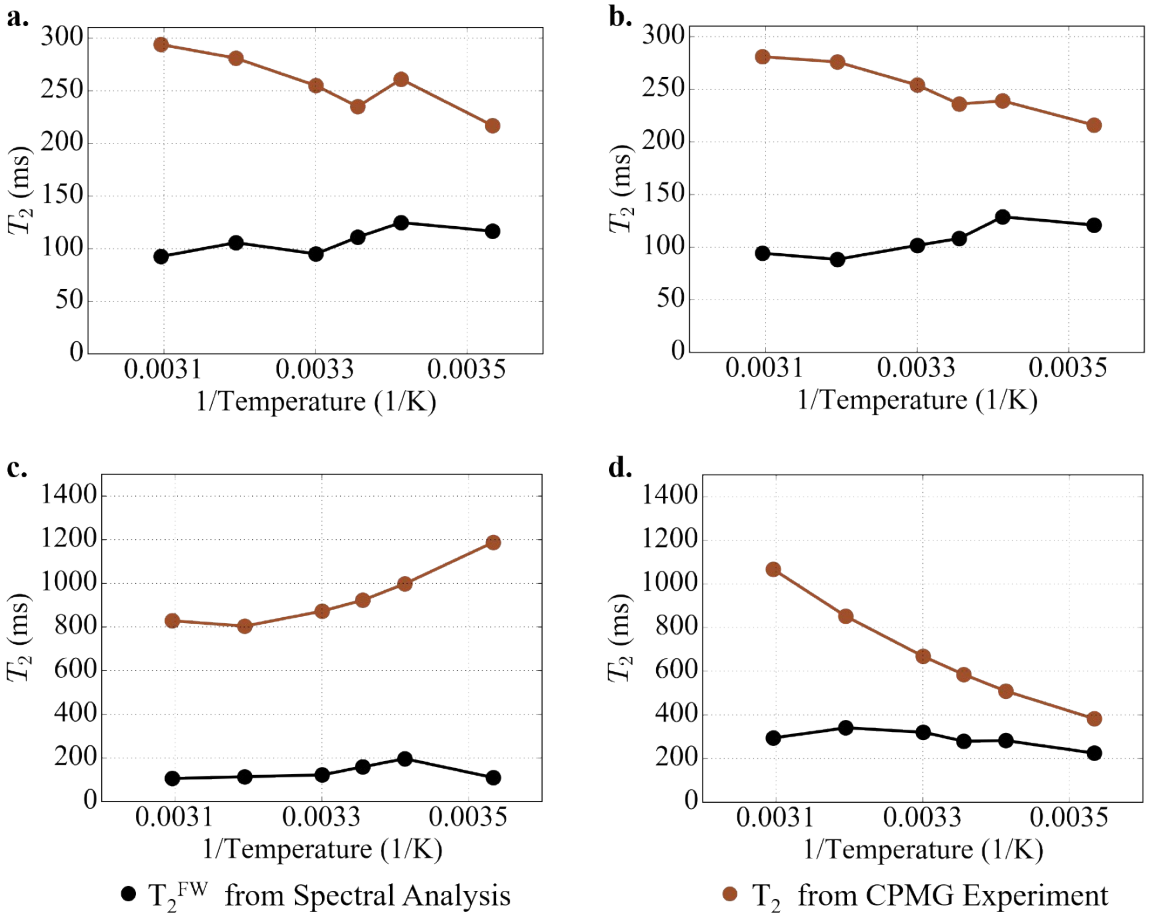

Figure S27. T_2^{FW} values from spectral analysis and T_2 values from CPMG for (a) DMF at 2.8 ppm, (b) DMF 3.0 at ppm, (c) residual ^1H in D_2O at 4.65 at ppm and (d) fraction **A** for a **VH** suspension at 3.69 ppm. This confirms comparable heterogeneous contributions to the line broadening in for resonance arising from free and NP-bound groups.

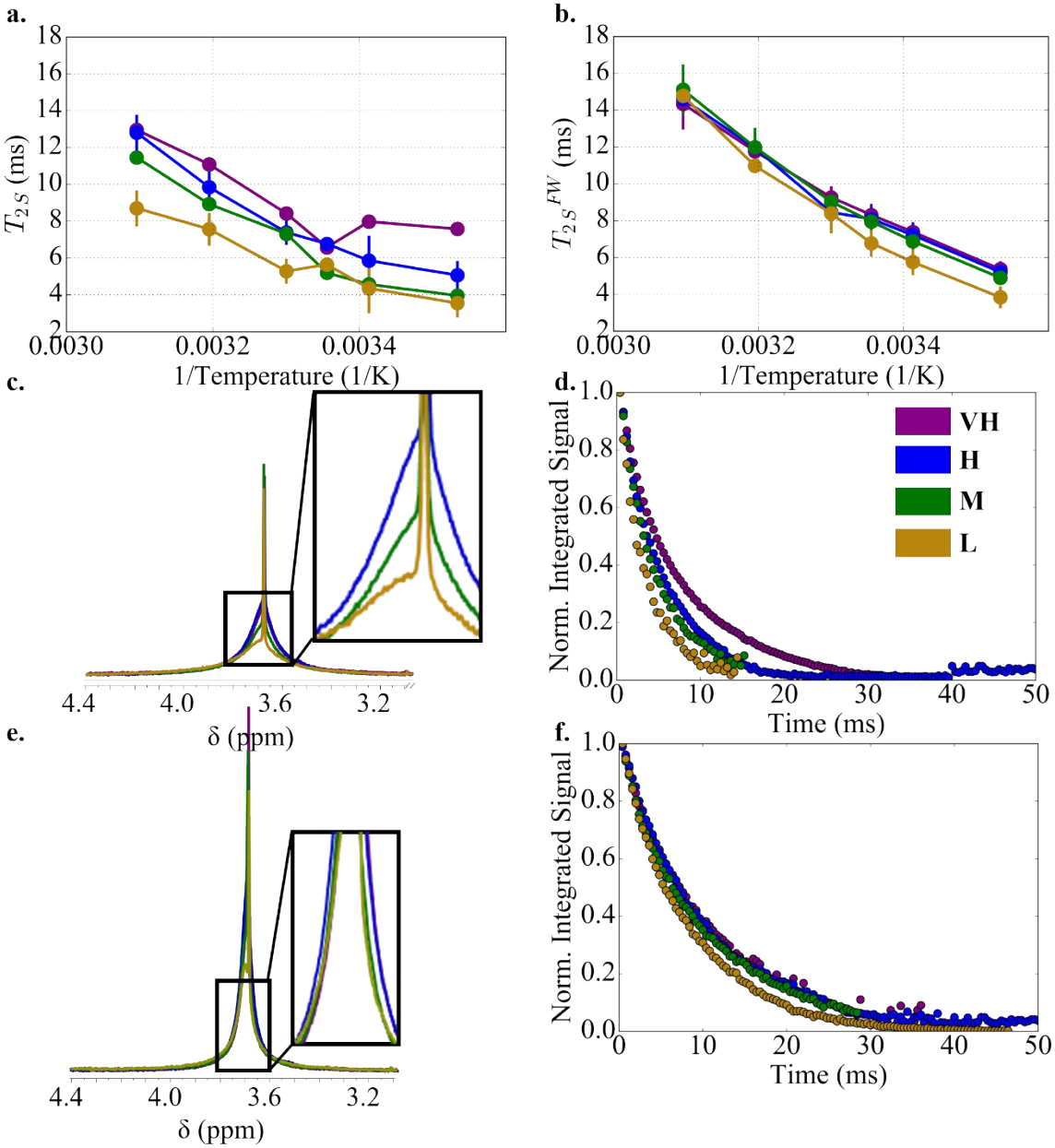

Figure S28. Comparison between (a) T_2 values for fraction ***B*** measured using CPMG, and (b) T_{2S}^{FW} from a two Lorentzian spectral analysis. The first echo of the CPMG experiment and the full integrated echo train for (c and d, respectively) 10°C and (e and f, respectively) 40°C highlight the difference in signal decay in the CPMG experiments. This demonstrates the insensitivity of the spectral analysis to variations in the lifetime, as discussed in the SI section below.

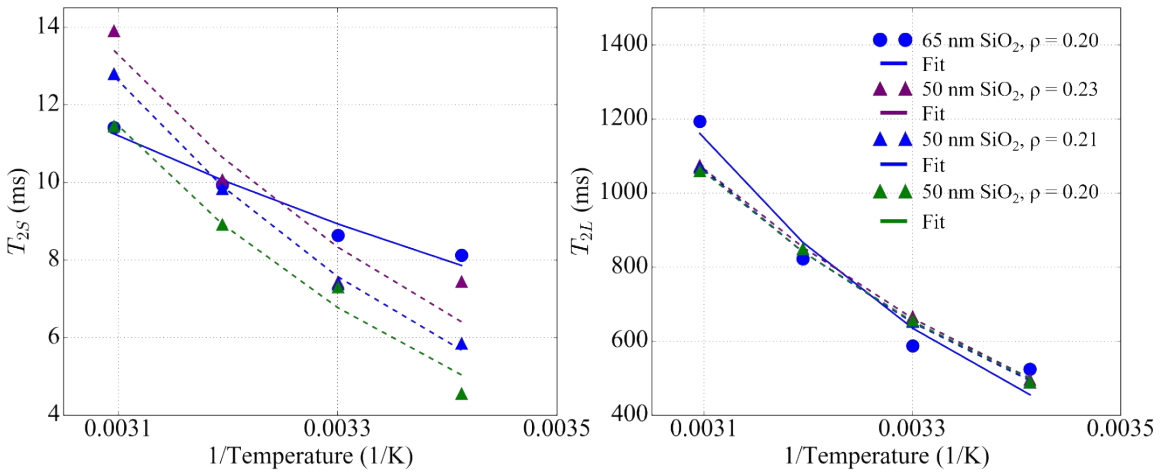

Figure S29. A comparison between the (a) T_{2S} and (b) T_{2L} values determined for PEG 5000 grafted onto 50 nm (triangles and dashed lines) and 65 nm (circles and solid lines) nanoparticles at similar coverage.

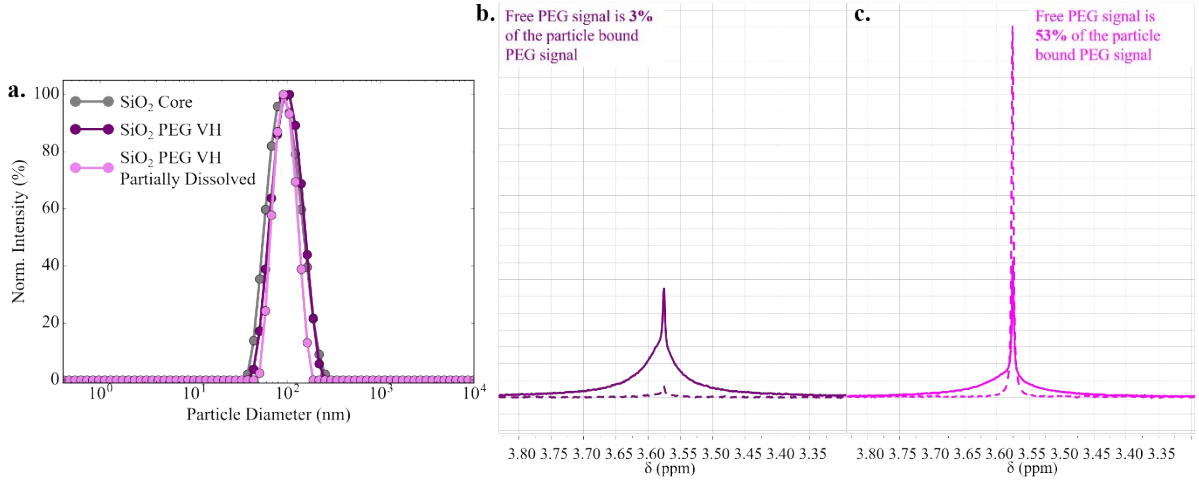

Figure S30. (a) DLS intensity distributions recorded for bare SiO_2 (grey), PEGylated SiO_2 (purple) and partially dissolved PEGylated SiO_2 (magenta) stage. Comparison between the free (dashed) PEG from the final supernatant and PEG peak on the particles (b) before and (c) after partial dissolution are also included. This confirms that particle dispersion is relatively unchanged during the rapid dissolution described in the main text.

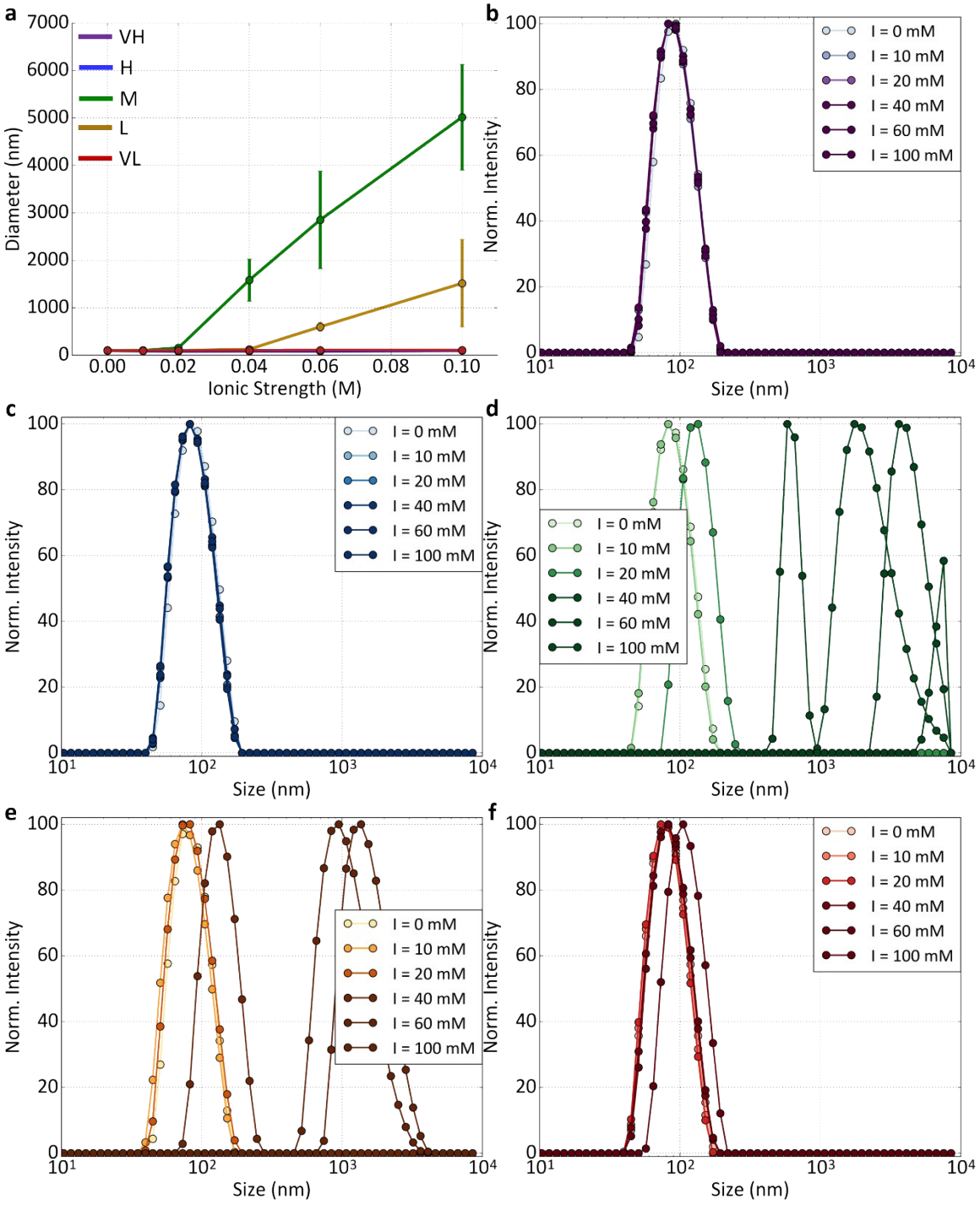

Figure S31. Colloidal stability of SiO_2 PEG_{5000} particles in solutions with increasing ionic strength expressed by (a) the mean hydrodynamic diameter averaged over N = 3 batches and representative spectra for (b) **VH**, (c) **H**, (d) **M**, (e) **L** and (f) **VL** particles.

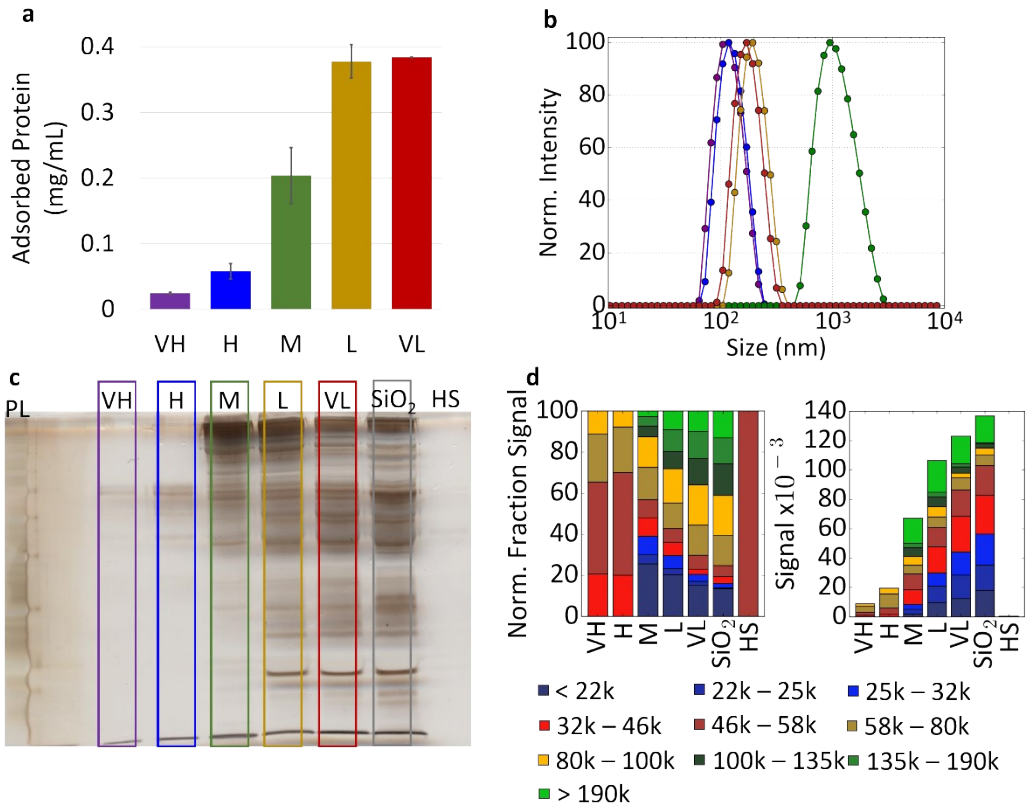

Figure S32. (a) Total amount of bound human serum protein to SiO_2 PEG **VH – VL** particles measured by micro BCA. (b) Size distribution of **VH – VL** particles during incubation with human serum. (c) Hard corona formed around SiO_2 and SiO_2 PEG **VH – VL** particles compared to human serum treated as a sample (i.e. gone through four washing cycles) and (d) representative gel analysis.

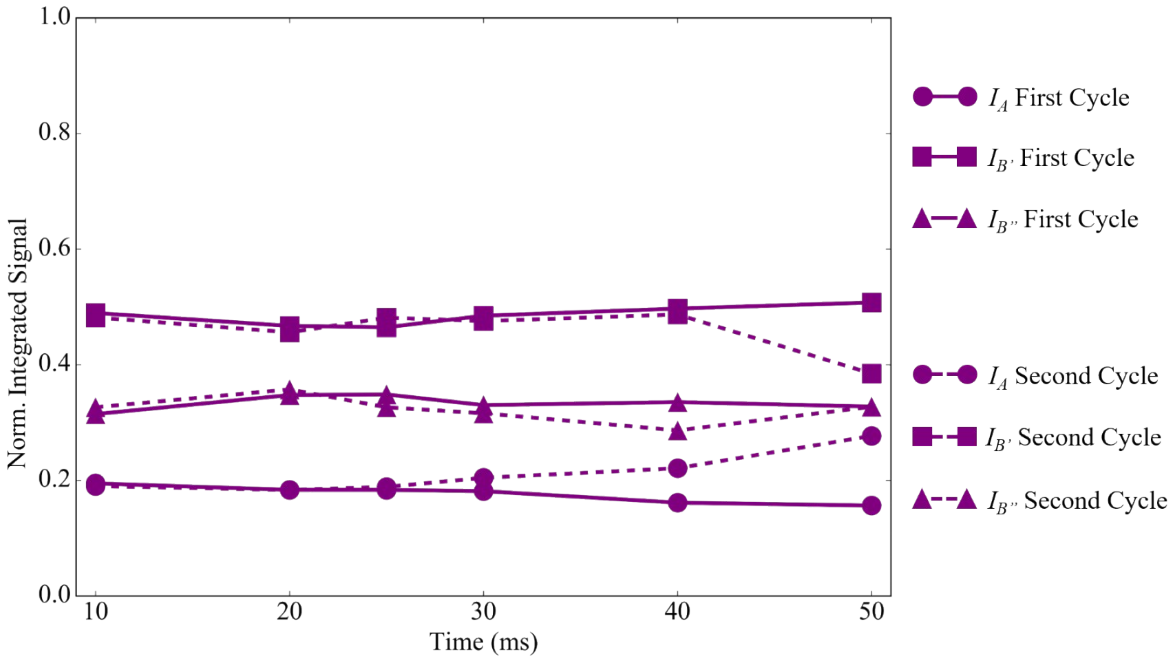

Figure S33. Normalised I_A, $I_{B'}$ *and* $I_{B''}$ values for representative ***VH*** spectra recorded over two heating cycles performed in consecutive weeks in the same order (10 to 50°C) and comparable conditions. This confirms the stability of the samples/analysis to temperature for the first cycle; all data shown in the manuscript was recorded during a first cycle.

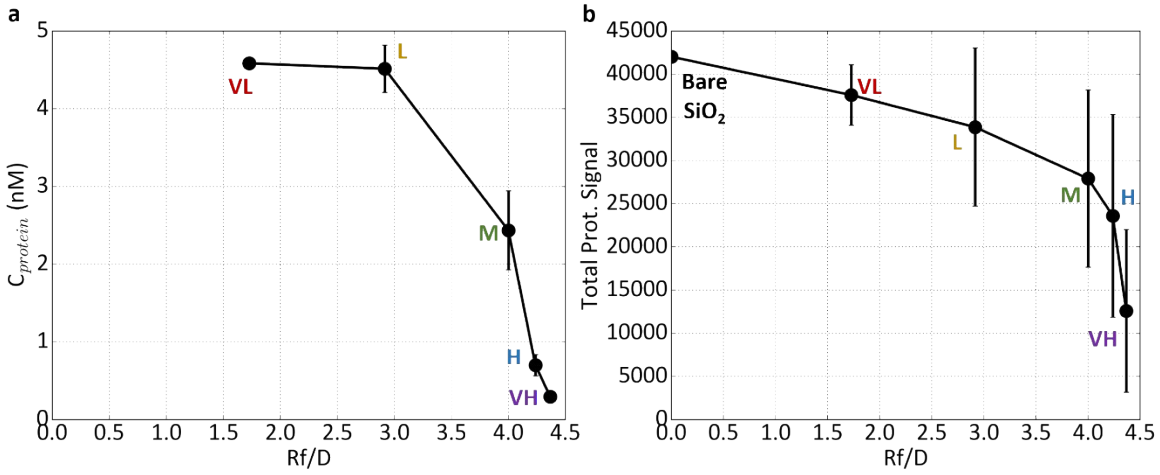

Figure S34. Trend between the Rf/D of the SiO2 PEG particles and the amount of proteins in the hard corona measured by (a) microBCA in mM and (b) grayscale signal integration from an SDS-PAGE gel. Image analysis done through ImageJ. MicroBCA results are an average of n = 2 independent samples while SDS-PAGE are averaged from four independent sample results.

Notes

Details on lineshape analysis

Lineshape fitting approaches using Mestrenova, Origin 8 and an in-house developed python script were compared. It was found that python script fitting was relatively accurate and more flexible. It also offered a distinct time advantage making the analysis of simple single ^{1}H NMR as well as relaxometry experiments with large numbers of echoes (> 1000) at different temperatures for the same sample using the same methodology possible. In rare cases a more visual analysis was preferred and thus Mestrenova was used. Origin 8 results were comparable to the script but the methodology was much slower and more limited.

The fractions contributing to the main resonance were quantified using all the following models; (i) 1 Lorentzian or Gaussian (ii) 2 Lorentzians, (iii) 3 Lorentzians, (iv) 4 Lorentzians, (v) 1 Lorentzian and 1 Gaussian, (vi) 1 Lorentzian and 2 Gaussians, and (vii) 2 Lorentzians and a Voigt transfer function (examples in figure S4). The resulting analysis is only weakly dependent on the model selected so long as > 90% of the signal is fitted. In no case did substituting of a Lorentzian for a Gaussian function improve the fit, furthermore moments analysis confirmed that the broader part of the resonance is not Gaussian in form.

Note that we also assessed the lineshape of the broader (***B***) component by second moments analysis after removing the ***A*** fraction. A line is often considered gaussian if the ratio of the moments, $S_4/S_2^2 = 3$, however we found a value > 4 in all cases. There are some approximations; as a Lorentzian does not have any defined moments during the calculations it is necessary to subtract the 1st moment (to obtain the moment referring to the centre). Despite the technical limitations of this approach it clearly demonstrates that there is no reason in the data for applying a Gaussian function to fraction ***B***.

The lineshapes of the ethylene resonance were analysed using a sum of Lorentzians. While it was possible to fit > 90% of the intensity using two Lorentzians, an almost perfect fit (R^2 > 99%) could be obtained by using three or more. The best fit with the fewest parameters was obtained using three Lorentzian functions (figure 1, S4) hence the fitting parameters; peak integral (*I*), FWHM and chemical shift, δ, were measured using this approach. It was found that the narrow part of the ^{1}H resonance is well represented by a single Lorentzian of integrated area, I_A, and the broadened part by two Lorentzians (***B'*** and ***B"***) which are summed to give its total integral, I_B, as shown in figure 1c. It is important to note that the analysis shown in figure 1 and particularly figure 2 is insensitive to the number of lines used in the analysis. This is demonstrated by the close similarity of alternative versions of figure 2, completed using different numbers of functions (figure S10). Further confirmation of the robustness of the methodology is provided by the samples **VH** and **H** in figure 2. Although a greater quantity of PEG was used in the grafting step for the former, the final coverage of these two samples is indistinguishable; presumably as it is close to the maximum possible under the conditions used. Encouragingly, the spectral response (figure 2b) and quantitative analysis (figure 2c, d) of these two samples which are effectively replicates, averaged from N = 3 in both cases, are almost identical.

Dependence of ^{1}H NMR spectra on NP size and chain length:

Changes in the NMR response with varying chain length and core size were studied (details in ESI) and were found to be consistent with the above picture.

The effect of reducing chain length to 1000 Da are shown in Figure 4g and h (main text). T_{2L} was found to be insensitive to chain length, indicating that the dynamics of fraction ***A*** are largely unchanged. The signal was much broader and with a less defined ***A*** fraction (figure

S6a), the SR value was also much lower at *c*.50% (figure S7b). The detectable intensity, I_{AB} , is reduced (Figures S5, S7) and the ratio I_A/I_B decreased (fewer unhindered units for shorter chains). We tentatively assign the changes in the temperature dependence of T_{2S}, Figure S28, to changes in the barrier to reorientation for ***B*** arising from reduced curvature. Hence the effect of shorter chains on the ^{1}H response, and underlying dynamics, is again consistent with the detailed analysis of the surface effects for PEG5000 grafted 50 nm NPs, presented in Figures 2a and 5. The data available strongly suggests that for all chain lengths studied the local dynamics, and hence the number of monomers contributing to fractions ***A***, ***B*** and ***C***, is determined by restrictions at the graft which are gradually relaxed along the chain depending on coverage.

The effect of increasing core size to 65 nm, while retaining the same PEG5000 coverage, is marginal, Figure S28. For larger particles sizes (100-200 nm) the spectral response is further broadened with gradual reduction in I_{AB} and I_A/I_B (Figure S7), and the dynamic information described for the sample presented here is gradually lost.The ^{1}H signal recorded for 80 and 95 nm particles contained two fractions but was relatively broader compared to that for 50 nm particles, while for 200 nm particle suspensions the signal was almost completely broadened into the background (figure S7a). SR values of *c*.80% were recorded for 50-100 nm which dropped to *c*.20% for 200 nm NP suspensions (figure S7b). The changes in the δ-value on increasing the NP size are minor, typically ≤ 0.03 ppm on increasing the size up to *c*.200 nm (figure S5b, e and h), resulting in only slight differences in the signal lineshape (figure S6 and S7). Changes in chemical shift on bonding have previously been attributed to (i) changes in hydrogen bonding to H_2O, (ii) associated with differences in average chain conformation,[1,2] (iii) electronic effects associated with the SiO_2 core may also become more important for the ethylene units close to the NP surface.

Long term stability of silica nanoparticles

The long term stability of silica nanoparticles is largely determined by the dynamic nature of the silica phase[3-5]. Slow dissolution at neutral pH [3] means that over time there is an increasing quantity of free PEG in the NP suspensions. Several authors have noted the importance of minimizing this interference hence we have increased the number of centrifugation cycles, beyond the recommended four [6]. We also measured the free PEG by analysis of the supernatant (following 5 centrifugation steps) immediately after the synthesis (figure S11) and twelve weeks later (figure S12).

Irreversible changes in the spectra and relaxation properties were observed after storage in an NMR tube at ~20°C after twelve weeks (figure S12b). Of particular note is the change in the signal remaining, this can be partially attributed to free PEG although the broader lineshape (as compared to figure S3) suggests some NP bound materials remains. This effect was noted early in the study and necessitated repeat preparations and acquisition of all data using at most two heating cycles (10 to 50 to 20°C) presented within a 6 week period, during which time the NMR spectral and relaxation responses were stable. Additionally, we have seen that the I_A/I_B trend is comparable in two consecutive heating cycles (figure S13), hence performing a cycle of variable temperature NMR did not stimulate any measurable desorption.

Hole-burning experiments:

To further investigate the broadening interactions, responsible for fraction ***B*** in particular, a series of hole-burning experiment was undertaken using a frequency selective RF pulse to irradiate at different δ-values across the main resonance. The results are shown in figure S14.

In all cases in which there is significant suppression of the signal it is not possible to burn a hole. In particular, when irradiated off center at 3.8 ppm ($\Delta\nu_{RF}$ = 15 Hz) most of the ***B*** fraction (δ_B = 3.70 ± 0.01 ppm, FWHM of ~ 30 Hz or 0.05 ppm) intensity was lost while the overlapping ***A*** fraction (δ_A = 3.69 ppm, FWHM of ~ 2 Hz or 0.003 ppm) remained largely unchanged (figure S14). On the other hand, when the narrow fraction was irradiated on center both fractions were greatly suppressed, leaving some fine structure discernable. This confirms that the two fractions are largely uncoupled and that fraction ***B*** is predominantly homogeneously broadened, presumably due to residual dipolar interactions. Note that the irradiation width is too large to make meaningful assumptions about heterogeneous contributions to the linewidth of fraction ***A*** which are discussed in the main text. These observations differ from the report of heterogeneous effects, described by Kohlmann et.al.,[7] for sub 3 nm Au NPs for which some of the broadening and asymmetry was attributed to the wide distribution of particle sizes. Finally, the residual intensity observed on irradiating ***A***, may arise from incomplete peak suppression, the small amount (*c.*1%) of free PEG noted above, and/or from a residual heterogeneously broadened ^{1}H contribution (*e.g.* arising from a tiny NP sub-population). In any case these observations confirm that these features are too weak to affect the quantification shown in figure 2.

Optimizing the relaxometry experiments and data analysis

T_1 inversion-recovery experiment

Three tau values, 5, 20 and 100 ms, were used to explore the T_1 relaxation over for 600 ms, 6000 ms and 10000 ms, respectively (figure S15 – S17). In all cases the signal shape was unchanged and both fractions passed through the null at similar tau values, *c.* 400 – 600 ms.

Thus signal fitting, using the two Lorentzian model discussed above, was applied to separate both signals and obtain the two T_1 values.

T_2 CPMG *experiment*

The 180^o pulse was calibrated prior to each CPMG experiment (figure S18). Five echo delays were tested 0.1, 1, 10, 50 and 100 ms (figure S19). Of those 0.1 and 10 ms captured the two fractions well, i.e. the intensities overlapped almost perfectly (despite the number of echoes), and so were used in the analysis (figure S20). Using a script developed in-house all spectra from the echo train were extracted and fitted to yield integrals for the fast and slowly relaxing fractions (see methods). Four approaches were compared:

- Manually integrating the peak in Mestrenova (I_{AB}) and fitting the resulting integrals with;
    - (i) two mono-exponential functions (one for the early and one for the later part of the echo train), or;
    - (ii) one bi-exponential function for the full train, or,
- Automatically integrating the peaks (using a python script) and fitting the resulting integrals with
    - (iii) two mono-exponential functions, or
    - (iv) one bi-exponential function, as in (i) and (ii).

It was found that the most consistent results were obtained from an automatic mono-exponential fit to each of the two stages (figure S21 and table S2) and this approach was used for all T_2 data presented.

Comparing T_{2S} results from linewidth analysis and CPMG experiments

For fraction ***B*** the T_{2S}^{FW} values (from spectral analysis) and the T_{2S} values (from CPMG) were in reasonable agreement as both are in the range of 3-15 ms (figure S25) indicating that fraction ***B*** is predominantly homogeneously broadened. This further supports the interpretation of the hole – burning experiments, as noted in the main text. It is our opinion that the minor discrepancies are due to: (i) insufficient sensitivity of the spectral analysis to moderate changes in the parameter representing the linewidth, e.g. ΔT_{2S} of 2 ms results from ΔFWHM of 6 Hz; (ii) comparatively higher precision of the CPMG analysis data, consisting of hundreds of echoes; (iii) reduced sensitivity of the echo analysis to initial fitting conditions and (iv) possible T_2 filtering of the broader fraction of the signal in a CPMG experiment. Thus, we consider the T_{2S} values measured through CPMG to be more accurate. It was found that the T_{2S} values decrease for reduced ρ (figure 4b). The only assumption made in analysing the CPMG echo trains was of exponential decays.

Evaluating changes in chain mobility with ligand and particle size

Evaluating the effect of PEG chain length on chain mobility is not trivial as it depends on the distance between molecules and their Flory radius. In this case while the chain coverage for long chains is much lower (ρ *c.*0.4 and *c.*0.9 nm^{-2} for PEG5000 and PEG1000, respectively for samples prepared from the same NP batch), their Flory radii are higher (figure S27). It was found that the T_{2S} value (fraction ***B***) was measurably smaller for the shorter PEG1000 chain compared to PEG5000, while T_{2L} was unchanged (figure 4g and h). This observation is consistent with the dynamics of fraction ***A*** being independent of the nanoparticle core and ligand inner structure, while fraction ***B*** being more sensitive to it and thereby a part of the ligand inner structure. Furthermore, the reduction in T_{2S}, i.e. more restricted movement, even at higher ρ for shorter PEG chains may be attributed to the longer average distance between

chains compared to their Flory radius thus allowing them to diffuse closer to the core particle (figure S27). This would explain why the signal is comparatively broad (figure S6) and its SR is lower (figure S7).

The variation of the PEG T_2 values with temperature was weakly dependent on NP size. The response of 50 and 65 nm PEG5000 grafted NPs, with comparable coverage, was measured, the data is shown in figure S28. Larger particles may show stronger temperature dependence of T_{2L} (fraction ***A***) and weaker dependence for T_{2S} fraction ***B***., but the effects are too weak over this size range to comment further.

Materials and Methods

Materials

Methanol (Sigma Aldrich Prod. Code: 34860), ammonia (36%, Fisher Scientific Prod. Code: a/3280/pb17), tetraethyl orthosilicate (TEOS, Sigma Aldrich Prod. Code: 333859), 1000 Da polyethylene glycol (NanoCS, Prod. Code: PG1-SL-1k), 5000 Da polyethylene glycol (Iris Biotech GmbH Prod. Code: PEG4795), deuterium oxide (Sigma Aldrich Prod. Code: 151882), dimethylformamide (DMF, Fischer Prod. Code: D13846117)

Methods

Particle synthesis and modification

70 nm and 90 nm Silica Nanoparticle Synthesis

70 and 90 nm particles were made the same way as 50 nm particles with the exception that 1 g and 1.2 g of ammonia (28.0–30.0% NH_3 basis) were used instead.

200 nm Silica Nanoparticle Synthesis

A detailed description of the 200 nm silica particles synthesis can be found in the SI of [8]. Briefly, 85 mL of methanol were dosed from a bottle to the reaction flask to which 25 mL of a 1 to 1 (V/V) methanol to ammonia and 7 mL of MiliQ water ware added. The mixture was closed and left to equilibrate for 10 minutes after which 3.5 mL of TEOS were added. It was sealed and left to react for an hour. The resulting 100 nm particles were allowed to undergo maturation for a further hour after which they was diluted by a factor of three with a 7.8 : 1 methanol : ammonia solution. TEOS was pipetted into the above dispersion at a rate of 1 mL

per 30 minutes until the particle size was measured to be 200 nm (characterized by DLS Number Mean). It is important to keep the particle concentration relatively low to minimize aggregation.

The dispersion was spun at 4000 (3220 rcf) rpm for 20 minutes, the supernatant was pipetted out and the particles were resuspended in ethanol once and water three further times. The final particle concentration was measured to be concentration of 65 mg mL^{-1}.

65 nm Silica Nanoparticle Synthesis

65 nm particles were synthesised using the same apparatus and general practices as for 200 nm particles and described in detail in the SI of [8].

Specifically a clean jacketed three necked flask was equipped with a 30 mm egg shaped magnetic stirrer and connected to a water bath with a build in pump (temperature was set at 40°C). After temperature equilibration 44 mL of methanol were added into the flask followed by 3.2 mL of an ethanol/ammonia solution with a 7:3 molar ratio and 3 mL deionised water. The mixture was left to equilibrate for ~10 minutes under constant stirring (~600 rpm) using a magnetic stirrer. TEOS (1.9 mL) was finally added to the vessel which was promptly sealed and left for 2 hours. The resulting particles were washed four times with water using centrifugation (13 500 rpm, 15 min) and characterised with DLS.

PEGylation of 70 and 90 nm Silica Nanoparticles

PEGylation of 70 and 90 nm particles was done in the same way as described in above, however, only **VH** PEG coverage was synthesised.

PEGylation of 200 nm Silica Nanoparticles

1 mL of 10 mg/mL 200 nm bare silica particles were spun at 3220 rcf for 20 minutes and redispersed in MiliQ water before reaction. The dispersion was heated to 90°C and allowed to equilibrate for 10 minutes while shaking at 1000 rpm. 5 kDa methylated PEG silicate was added to the particles in a concentration of 10 (**VH**), 1 (**H**), 0.25 (**M**), 0.1 (**L**) and 0.01 (**VL**) PEG/nm^2. The dispersions were left to react in this way for one hour after which they were washed four times in the same manner described above.

Partial dissolution of SiO_2 - PEG VH.

70 µL of PBS was added to 0.7 mL of SiO_2 PEG **VH** particles (5 mg/mL) in D_2O 1 mM DMF water (I = 1.4 mM) in a 2 mL Safe Lock © eppendorf. The dispersion was heated up to 37°C and left to incubate for 1 h. Particles were spun down once (13 500 rpm, 15 min) and resuspended in 1 mM DMF in D_2O. Both the supernatant and particle dispersions were kept and measured in NMR. The latter was measured in DLS and TEM, and compared to the previous particle stages.

Particle characterisation

Size by Dynamic Light Scattering (DLS)

A Malvern Zetasizer ZS series was used in all measurements. Bare and PEGylated silica particles were diluted in water as 1 in 100 for a final concentration of ~100 μg/mL in a plastic low volume cuvette (PLASTIBRAND, semi-micro, PMMA, l = 1 cm). Each measurement was conducted at least three times and consisted of 11 consecutive 10 s runs at 25°C. There was no equilibration time prior to experiment.

Zeta Potential

After the size measurement particles were transferred to a zeta potential cuvette (Malvern Panalytica, Prod. Code: DTS1070) and measured three times using 11 consecutive runs each. The zeta potential presented is an average of those measurements. All measurements used the Smoluchowski model. If needed 10 μL of PBS was added to the particle dispersion to increase its conductivity to ~0.1 mS/cm. There was no equilibration time prior to experiment.

Transmission electron microscopy (TEM)

Silica particles were diluted to a concentration of 100 μg/mL with water; 10 μL were transferred son a Formvar carbon 200 mesh copper TEM grid (Agar Scientific, Prod. Code: 01801) and left to dry in air overnight. The grid was imaged using FEI Tecnai 120 instrument using 120keV.

NMR Experiments

^{1}H NMR at various temperatures

Samples as prepared were run after stabilising the temperature for 30 minutes. An experiment to determine the ^{1}H pulse was run before running an inverse recovery experiment, then we run a proton experiment. Spectra were recorded with a hard 45^o ^{1}H pulse of duration 3.20 μs, relaxation delay of 25 s, acquisition time of 5.0 s, number of scans was 16, tof at -215.95 Hz (4.64 ppm), processing with 48K points and no weighting function applied before the Fourier Transformation.

Signal inversion recovery experiment, T_1

Samples as prepared as described above were run after stabilising the temperature during 30 minutes. An experiment to determine the ^{1}H pulse was run before running an inverse recovery experiment. "T1 Inverse Recovery" experiments were run using a hard 90 degrees ^{1}H pulse of duration 6.40 μs, relaxation delay of 30 s, acquisition time of 5.0 s, number of

scans of 4, tof at -215.95 Hz (4.64 ppm), the array relaxation delay d2 was arrayed 100 times from 0.1s with 0.1s step, processing with 48K points and no weighting function applied before the Fourier Transformation.

CPMG experiment, T_2

Samples as prepared above were run after stabilising the temperature over 30 minutes. An ^{1}H pulse length was calibrated before running the CPMG experiments. "Carr-Purcell Meiboom-Gill T2" was run with a hard 90^o ^{1}H pulse of duration 6.40 μs, relaxation delay varied with temperature, an acquisition time of 5.0 s, number of scans of 4, tof at -215.95 Hz (4.64 ppm), for a fixed tau value and with a big tau value which was arrayed 300 times from 0.0004 s with 0.0004 s step, processing with 48K points and no weighting function applied before the Fourier Transformation. Different Tau values are shown in Table S3.

Table S4. Echo delay (Tau, τ) and delay between echo recording (Big Tau, Big τ) in all CPMG T_2 experiments. τ_1 corresponds to T_{2S} while τ_2 corresponds to T_{2L}.

T(°C)	Sample	τ_1 (ms)	Big τ_1 (ms)	τ_2 (ms)	Big τ_2 (ms)	Cycle Time (ms)
10	**VH** PEG Coverage	0.1	0.4	10	40	15000
	H PEG Coverage	0.1	0.4	5	10	5000
	M PEG Coverage	0.1	0.4	5	10	5000
	L PEG Coverage	0.1	0.4	5	10	5000
20	**VH** PEG Coverage	0.1	0.4	7	14	7000
	H PEG Coverage	0.1	0.4	7	14	7000
	M PEG Coverage	0.1	0.4	7	14	7000
	L PEG Coverage	0.1	0.4	7	14	7000
25	**VH** PEG Coverage	0.1	0.4	10	20	10000
	H PEG Coverage	0.1	0.4	10	20	10000
	M PEG Coverage	0.1	0.4	10	20	10000
	L PEG Coverage	0.1	0.4	10	20	10000
30	**VH** PEG Coverage	0.1	0.4	8	16	10000
	H PEG Coverage	0.1	0.4	9	18	10000
	M PEG Coverage	0.1	0.4	10	20	10000

	L PEG Coverage	0.1	0.4	10	20	10000
40	**VH** PEG Coverage	0.1	0.4	10	20	10000
	H PEG Coverage	0.1	0.4	12	24	15000
	M PEG Coverage	0.1	0.4	14	28	15000
	L PEG Coverage	0.1	0.4	14	28	15000
50	**VH** PEG Coverage	0.1	0.4	10	40	20000
	H PEG Coverage	0.1	0.4	10	40	20000
	M PEG Coverage	0.1	0.4	10	40	20000
	L PEG Coverage	0.1	0.4	10	40	20000

Hole burning experiments

PEGylated samples were run after stabilising the temperature during 30 minutes. An experiment to determine the ^{1}H pulse was run before running an inverse recovery experiment then PRESAT experiments were run using a 45 degrees hard pulse of duration 3.20 us, an acquisition time of 5s, a relaxation delay of 25s with 16 scans with a spectrum window of 16 ppm center on the water signal at 4.64 ppm (tof = -215.95 Hz). The width of the size-selective pulse was determined by the power of the RF field used (presaturation power -8 dB / 15 Hz) the pulse was applied for 2s. Processing was with 48K points and no weighting function was applied before the Fourier Transformation.

NMR signal analysis

The MastReNova 11.0 was used to process all obtained spectra. All spectra were referenced, phase corrected (if required), baselined, and an exponential apodization of 0.3 Hz was applied. All baselining was done using a 3 parameter Polynomial Fit.

Calculations and Signal Fitting

Particle mass and concentration calculation

Particle mass was measured using either a balance with a readability of 0.1 mg (for all silica core particles) or 0.1 µg (for most presented PEGylated particles). A volume (typically ~200 µL) of particles were pipetted into a new HPLC glass vial and dried overnight using a vacuum oven. After which the vials were taken out, their entrance was covered with paper or tin foil and left to equilibrate to room temperature for at least 3 h. Each vial was weighted a minimum of three times before and after drying.

Sample surface area calculation

Several assumptions were made when calculating the sample surface area:

- All particles are perfect, solid spheres of the same size.
- The density of the silica in the particles is 2 g/mL.
- The Number Mean diameter of the dispersion accurately represents the physical size of the particles in a good dispersion.

In this case the total surface area of a sample was calculated as:

$$Total\,SA = N_{NP} \times 4\pi r^2, \qquad \text{Eq 1}$$

where r is the Number Mean radius of the particles as obtained from the DLS and N_{NP} is the calculated number of particles, defined below.

$$N_{NP} = \frac{3}{4} \times \frac{m \times 10^{18}}{\pi \times r^3 \times d}, \qquad \text{Eq 2}$$

where r is the Number Mean radius of the particles as obtained from the DLS, m is the dry mass of the sample in mg and d is the density of silica. The factor 10^{18} is to convert nm^3 to μL.

PEG addition calculation

In this work the particle types are defined by a specific PEG.nm^{-2} ratio added during the modification step. Those were calculated as:

$$m\,(PEG) = i \times \frac{Total\,SA}{N_A} \times M \times 10^3, \qquad \text{Eq 3}$$

where i is the number of PEG.nm^{-2} of the desired particle type (5 for **VH**, 2.5 for **H**, etc.), $total\,SA$ is as defined in eq 1, N_A is Avogadro's number, $M$is the molar mass of the used PEG and the 10^3 is to convert the result to mg.

PEG coverage calculation

PEG coverage was determined by weighing (to four decimal places-readability, 0.1 mg, or seven decimal places-readability, 0.1 µg, as appropriate) the dry powders, with subsequent re-dissolution of the particles in 0.2 M NaOH in D_2O. The ^1H spectrum of the solution was then used to determine the total PEG amount and thereby ρ using the previously described procedure (ref 24 main text). calculated by dissolving a particle sample in 0.2 M NaOH, measuring the now molecular PEG in NMR, normalizing the signal integral to an internal standard (1 mM DMF) and comparing the corrected integral to a calibration curve.

Measuring PEG calibration curves

PEG 5000

Silicate PEG 5000 OMe at a concentration of 4.2 mg/mL (8.4×10^{-1} mM), 1.55 mg/mL (3.1×10^{-1} mM), 0.78 mg/mL (1.56×10^{-1} mM), 0.34 mg/mL (6.8×10^{-2} mM), 0.17 mg/mL (3.4×10^{-2} mM) was dissolved a 1 mL solution of 200 mM NaOH with 1mM DMF as an internal standard. The solution was left overnight at 37^0C to match dissolution conditions and the measured. Accumulation time in the measurement was 10 seconds and each measurement consisted of 32 scans. Two calibration curves were averaged. The mean PEG peak (3.6 ppm) was used to determine concentrations for the calibration curve.

PEG 1000

In a similar fashion PEG 1000 was dissolved in D_2O (200 mM NaOH, 1 mM DMF) at a concentration of 5 mg/mL (5 mM), 2.5 mg/mL (2.5 mM), 0.625 mg/mL (6.25×10^{-1} mM), 0.313 mg/mL (3.13×10^{-1} mM).

The intercept of both calibration lines was set to 0. The resulting fitting trend had a $R^2 > 0.99$.

Particle dissolution in NaOH

In a typical experiment 1 mL of D_2O (200 mM NaOH, 1 mM DMF) was added to the dry particles resulting from the mass measurement. The resulting suspension was sealed and left at 4 h at 40°C or overnight at 20°C.

Alternatively a volume of 5 – 6 M NaOH in D_2O and DMF were added to the particle dispersion which was then sealed and left in the same conditions as above.

Calculating the PEG.nm^{-2} in a sample.

PEG coverage was calculated as:

$$PEG.nm^{-2} = \frac{N_{PEG}}{Total\ SA}, \qquad \text{Eq 4}$$

where N_{PEG} is the number of PEG molecules in the sample after dissolution obtained as explained above and the $Total\ SA$ is the total surface area of the sample.

Fitting

For T_1 measurements

T_1 measurements were conducted by acquiring 100 consecutive spectra which were fit by a two Lorentzian model. Importantly the fitting model used did not have a significant impact

on the final result. The as-obtained integrals were plotted as a function of recovery time and fitted using a monoexponential function as shown in eq 5.

$$M(t) = M_0(1 - e^{\frac{t}{T_1}}) \quad \text{Eq 5}$$

Where M_0 is a measure of the equilibrium magnetisation and t is the time in s.

For T_2 measurements

T_2 measurements were conducted by acquiring 300 consecutive spectra. The peaks were fit manually in the MaestreNova software, automatically using a two Lorentzian model and separating out the two signal modes. Similarly to above the fitting model had minimal effect on the final result. In some cases the 0.1 ms and 10 ms results were summed in one continual curve prior to fitting. Depending on data treatment the integration curves were fit with either a monoexponential (eq 6) or bi-exponential (eq 7) decay as demonstrated in figure S21.

$$y = y_0 + Ae^{-\frac{t}{T_2}} \quad \text{Eq 6}$$

$$y = y_0 + A_1e^{-\frac{t}{T_2{}^1}} + A_2e^{-\frac{t}{T_2{}^2}} \quad \text{Eq 7}$$

Where y_0 is a fitting factor (offset), $A, A_1$and A_2 are a measure of the magnetisation and x is the time in s. The results of various approaches to the data fitting are shown in table S2.

Calculating T_2 through signal lineshape analysis

T_2 can be calculated using the FWHM of the ^{1}H PEG signal using eq 9:

$$T_2 = \frac{1}{\pi\nu_,} \quad \text{Eq 9}$$

where T_2 is the relaxation time in s and ν is the FWHM of the peak in Hz. The FWHM was obtained by fitting the peak using the in – house python script as described above. Models used were; one Lorentzian for water and DMF, a sum of three Lorentzians for the PEG signal.

1 Balevicius, V. & Aidas, K. Temperature Dependence of 1 H and 17 O NMR Shifts of Water: Entropy Effect. *Applied Magnetic Resonance* **32**, 363-376 (2007).
2 Baxter, N. J. & Williamson, M. P. Temperature dependence of 1 H chemical shifts in proteins. *Journal of biomolecular NMR* **9**, 359-369 (1997).
3 Mahon, E., Hristov, D. R. & Dawson, K. A. Stabilising fluorescent silica nanoparticles against dissolution effects for biological studies. *Chemical Communications* **48**, 7970-7972 (2012).
4 Meder, F. *et al.* Labeling the structural integrity of nanoparticles for advanced in situ tracking in bionanotechnology. *ACS nano* **10**, 4660-4671 (2016).
5 Schneider, M. *et al.* Physicochemical properties and biodegradability of organically functionalized colloidal silica particles in aqueous environment. *Chemosphere* **99**, 96-101 (2014).
6 Liu, X., Yu, M., Kim, H., Mameli, M. & Stellacci, F. Determination of monolayer-protected gold nanoparticle ligand–shell morphology using NMR. *Nature communications* **3**, 1182 (2012).
7 Kohlmann, O. *et al.* NMR diffusion, relaxation, and spectroscopic studies of water soluble, monolayer-protected gold nanoclusters. *The Journal of Physical Chemistry B* **105**, 8801-8809 (2001).
8 Hristov, D. R. *et al.* Using single nanoparticle tracking obtained by nanophotonic force microscopy to simultaneously characterize nanoparticle size distribution and nanoparticle–surface interactions. *Nanoscale* **9**, 4524-4535 (2017).